Ozone Anomalies in the Free Troposphere during the COVID-19 Pandemic

Idir Bouarar[1], Benjamin Gaubert[2], Guy P. Brasseur[1], Wolfgang Steinbrecht[3], Thierno Doumbia[4], Simone Tilmes[2], Yiming Liu[5], Trissevgeni Stavrakou[6], Adrien Michel Deroubaix[1], Sabine Darras[7], Claire Granier[8], Forrest Gerhart Lacey[9], Jean-François Müller[10], Xiaoqin Shi[1], Nellie Elguindi[11], and Tao Wang[12]

[1]Max Planck Institute for Meteorology
[2]National Center for Atmospheric Research (UCAR)
[3]Deutscher Wetterdienst
[4]Laboratoire d'Aerologie, University de Toulouse, CNRS, UPS
[5]Sun Yat-sen University,
[6]Royal Belgian Institute for Space Aeronomy
[7]Observatoire Midi-Pyrenees
[8]University of Toulouse
[9]National Center for Atmospheric Research
[10]Royal Belgian Institute for Space Aeronomy (BIRA-IASB)
[11]Centre national de la recherche scientifique
[12]The Hong Kong Polytechnic University

November 24, 2022

Abstract

Using the CAM-chem Model, we simulate the response of chemical species in the free troposphere to changes in emissions of primary pollutants during the COVID-19 pandemic. Zonally averaged ozone concentrations in the free troposphere during Northern Hemisphere spring and summer were 5 to 15 % lower than 19-year climatological values, in good quantitative agreement with ozone observations. About one third of this anomaly is attributed to the drastic reduction in air traffic during the pandemic, another third to reductions in surface emissions, the remainder to 2020 meteorological conditions, including the exceptional springtime Arctic stratospheric ozone depletion. The overall COVID-19 reduction in mean northern hemisphere tropospheric ozone in June is less than 5 ppb below 400 hPa, but reaches 8 ppb at 250 hPa. In the Southern Hemisphere, COVID-19 related ozone reductions by 4 to 6% were masked by comparable ozone increases due to other changes in 2020.

Ozone Anomalies in the Free Troposphere during the COVID-19 Pandemic

Idir Bouarar[1], Benjamin Gaubert[2], Guy P. Brasseur[1,2,9], Wolfgang Steinbrecht[3], Thierno Doumbia[4], Simone Tilmes[2], Yiming Liu[6], Trissevgeni Stavrakou[7], Adrien Deroubaix[1], Sabine Darras[5], Claire Granier[4,8], Forrest Lacey[2], Jean-François Müller[7], Xiaoqin Shi[1], Nellie Elguindi[4] and Tao Wang[9]

[1]Environmental Modeling Group, Max Planck Institute for Meteorology, Hamburg, Germany, [2]Atmospheric Chemistry Observations and Modeling Laboratory, National Center for Atmospheric Research, Boulder, CO, [3]Deutscher Wetterdienst, Hohenpeißenberg, Germany, [4]Laboratoire d'Aérologie, Université de Toulouse, CNRS, UPS, France, [5]Observatoire, Midi-Pyrénées, Toulouse, France, [6]School of Atmospheric Science, Sun Yat-sen University, Guangzhou, China, [7]Royal Belgian Institute for Space Aeronomy, Brussels, Belgium, [8]NOAA Chemical Sciences Laboratory/CIRES, University of Colorado, Boulder, CO., [9]Department of Civil and Environmental Engineering, The Hong Kong Polytechnic University, Hong Kong China.

Corresponding author: Guy P. Brasseur (guy.brasseur@mpimet.mpg.de)

Abstract

Using the CAM-chem Model, we simulate the response of chemical species in the free troposphere to changes in emissions of primary pollutants during the COVID-19 pandemic. Zonally averaged ozone concentrations in the free troposphere during Northern Hemisphere spring and summer were 5 to 15 % lower than 19-year climatological values, in good quantitative agreement with ozone observations. About one third of this anomaly is attributed to the drastic reduction in air traffic during the pandemic, another third to reductions in surface emissions, the remainder to 2020 meteorological conditions, including the exceptional springtime Arctic stratospheric ozone depletion. The overall COVID-19 reduction in mean northern hemisphere tropospheric ozone in June is less than 5 ppb below 400 hPa, but reaches 8 ppb at 250 hPa. In the Southern Hemisphere, COVID-19 related ozone reductions by 4 to 6% were masked by comparable ozone increases due to other changes in 2020.

Plain Language Summary

The reduction in the emissions of primary air pollutants during the 2020 COVID-19 pandemic has generated perturbations in the chemical state of the atmosphere. A global Earth system model that accounts for chemical, physical and dynamical processes in the atmosphere and for the coupling between the atmosphere, the ocean and the land surface, indicates that the abundance of tropospheric ozone was significantly reduced during the pandemic in response to reduced emissions of primary pollutants associated with restrictions of air traffic and economic activities. These findings are consistent with observed ozone anomalies during the summer of 2020.

Major Findings

1. The ozone concentration in the northern extratropical free troposphere was 5 to 15% lower in May and June 2020 relative to climatology.

2. A third of this anomaly is attributed to meteorological conditions including stratospheric Arctic air with abnormally low ozone.

3. The reduction in surface and aircraft emissions associated with the COVID-19 pandemic has caused an ozone anomaly of 4 to 8%.

1. Introduction

The reduction in the emissions of primary pollutants during the COVID-19 pandemic, due to the worldwide slowdown in economic activity, produced a perturbation in the formation of secondary compounds, including ozone, and in the oxidative capacity of the lower atmosphere. Several studies have highlighted that the sign and magnitude of the anomaly depended on the photochemical regime in the region under consideration (Miyazaki et al., 2020; Le et al., 2020; Venter et al., 2020; Cazorla et al., 2020; Gaubert et al., 2021). In China, for example, where a strict lockdown was imposed as early as January 2020, the surface concentration of ozone increased in the North China Plain and in the major cities of the country (Shi and Brasseur, 2020, Huang et al., 2020; Liu et al., 2020; Miyazaki et al. 2020; Gaubert et al., 2021). In these NO_x saturated regions, the titration of ozone by nitrogen oxides was reduced during the entire lockdown period. In contrast, in the rural areas of southern China, which are NO_x-controlled, the surface concentration of ozone decreased during the pandemic (Liu et al., 2020; Lian et al., 2020). In the rest of the world, where the most stringent containment measures were introduced only in March and April 2020, the concentrations of surface ozone in remote areas were generally reduced (Weber et al., 2020; Gaubert et al., 2021) with positive anomalies mostly driven by meteorological conditions (Ordoñez et al., 2020).

Most of the early data analyses about the effect of the pandemic on air quality have focused on chemical species anomalies at the Earth's surface and were based on measurements from monitoring stations (Huang et al., 2020; Shi and Brasseur, 2020) and, for a limited number of species (e.g., nitrogen dioxide), on information deduced from satellite observations (e.g., the Tropospheric Monitoring Instrument, TROPOMI) (Bauwens et al., 2020). Little information on

the effects of the chemical perturbations during the COVID-19 pandemic in the free troposphere is currently available. A recent study (Steinbrecht et al., 2021) based on ozone measurements by balloon-borne ozone sondes as well as ground-based FTIR and LIDAR systems during the period 2000-2020 at latitudes 82.5^0N to 54.5^0S reported changes of free tropospheric ozone related to the COVID-19 disruptions. It shows that, from April to August 2020 and from 1 to 8 km altitude, the average concentration of ozone was 7% lower than the climatological mean values across most of the Northern Hemisphere.

To help interpret the reduced ozone concentrations, we use the global Community Atmosphere Model with chemistry (CAM-chem) and quantify the relative importance of the different processes that have contributed to the observed ozone anomalies. Unlike the situation in the boundary layer where the lifetime of ozone is of the order of a few days (Goldberg et al., 2015), the timescales associated with the temporal evolution of odd oxygen ($O_x = O_3 + NO_2$) in the free troposphere are of the order of several weeks (Stevenson et al., 2006), or even several months (Bates and Jacob, 2020) if one includes hydrogenated compounds (HO_x and its chemical reservoirs) in the definition of O_x. The behavior of ozone in the free troposphere therefore depends both on photochemical processes and on the effect of transport due to the atmospheric circulation.

During the year 2020, several events potentially affected ozone in the free troposphere: (1) the intense world-wide disruption of the surface emissions of primary pollutants in response to the COVID-19 pandemic; (2) the related reduction in air traffic with a reduced injection of NO_x, SO_2 and black carbon (BC) into the upper troposphere; (3) the particularly intense depletion of ozone in the lower Arctic stratosphere due to the abnormally stable and vigorous polar vortex during the first months of 2020 (Manney et al., 2020; Wohltmann et al., 2020; Inness et al., 2020, Wilka et al. 2021), (4) the interannual variability associated with meteorology, lightning and fires.

Here, we quantify the response of free tropospheric ozone to the aforementioned potential causes of the 2020 ozone anomaly by performing several sensitivity simulations in which the different sources of disturbances are taken into account. We compare the simulated overall responses with observed ozone anomalies from Steinbrecht et al. (2021).

2. Model description and overview of simulations

For the simulations reported in this letter, we use the Community Earth System Model (CESM) version 2.2 described by Danabasoglu et al. (2020) and adopted by Gaubert et al. (2021). The atmospheric component of the model (CAM-chem) provides a comprehensive description of atmospheric chemistry and aerosol processes (Gettelman et al., 2019; Tilmes et al., 2020; Emmons et al., 2020; Gaubert et al., 2020), at a spatial resolution of 1.25° in longitude by 0.95° in latitude (about 100 x 100 km^2 at mid-latitude), and with 32 vertical pressure layers from the surface to 2.6 hPa (about 40 km altitude). We adopt the MOZART Troposphere Stratosphere (TS1) chemistry mechanism (Emmons et al., 2020), which includes 221 gas phase and aerosol species and 528 chemical and photochemical reactions. Aerosol concentrations and size distribution are derived from the four-mode Modal Aerosol Model (MAM4, Liu et al., 2016; Mills et al., 2016). In order to realistically represent meteorological conditions for the period under consideration, the wind velocity components and the temperature are nudged at every physical step (30 min) towards the MERRA-2 meteorological analysis (Gelaro et al., 2017) with a Newtonian relaxation of about 6 hours. Figure S1 shows the calculated zonally mean of NO_x and ozone concentrations averaged over the month of 2020 (baseline case). Wilka et al. (2021) suggested to increase the nitric acid trihydrate (NAT) particle number density to increase the denitrification rate and reduces O_3. They found a better agreement with observations for both nitric acid and O_3. We use their suggested particle number density of 10^{-5} in a sensitivity experiment, giving an upper bound for stratospheric ozone reduction.

Anthropogenic surface emissions are based on the CAMS-GLOB-ANT_v4.2-R1.1 global inventory (Granier et al., 2019, Elguindi et al., 2020). Three-dimensional aircraft emissions are based on Hoesly et al. (2018). Biogenic emissions are calculated online from the Model of Emissions of Gases and Aerosols from Nature (MEGAN v2.1; Guenther et al., 2012). Daily

biomass burning emissions are based the Quick-Fire Emissions Dataset (QFED; Darmenov and Da Silva, 2014) include, for example, the 2019/2020 large fires in California, Colorado and Australia. Deposition of gases and aerosols are calculated through an active coupling between the atmosphere and the Community Land Model version 5 (CLM5; Lawrence et al., 2019). To account for the effect of the COVID-19 lockdowns, anthropogenic emissions are modified for each economic activity sector (industrial, mobility, residential, energy) and geographical region according to the CONFORM dataset developed by Doumbia et al. (2021) (see Supplementary Information and Figure S2). The reduction in the emissions by air traffic is estimated to be close to 80% between April and June. The different model simulations performed for the present study are summarized in Table S1.

We present here the calculated anomalies in the concentration of chemical species in the troposphere during year 2020 relative to a baseline case in which the COVID-related changes in the emissions are ignored. These numerical experiments only quantify changes due to the anthropogenic emissions following lockdowns across the world. We analyze the atmospheric response for three different cases: changes only in the surface emissions during the pandemic (case 1); changes only in the air traffic emissions (case 2) and the combined effects (case 3). We focus on the monthly mean changes in the global distribution of NO_x and ozone in a global domain extending from the surface to the lower stratosphere and from pole to pole. In addition, we assess the contribution of inter-annual atmospheric variability including the influence of the exceptionally high ozone depletion inside the 2020 Arctic vortex by comparing the baseline 2020 results (no COVID related effects included) with 2001-2019 climatology (case 4). Finally, we perform a comparison similar to case 4, but with the year 2020 simulation accounting also for the reduced anthropogenic emissions during the pandemic (case 5). This last case can be compared with the results of Steinbrecht et al (2021), in which observed ozone concentrations in 2020 are contrasted to the observed ozone climatology.

3. Results

Figure 1 shows the response of the zonally and monthly averaged ozone concentration due to the perturbed emissions (COVID-19, case 3) relative to the baseline case in which no lockdown

effect is applied to the emissions. We note the gradually larger reduction in the ozone concentration as time proceeds and photochemical activity increases; the relative anomaly does not exceed 2% in March, but reaches 7 % in May and June before it slightly decreases in July. While the lockdown measures were stricter in the Northern Hemisphere winter and spring 2020, the photochemical response of ozone was largest in summer. The relative changes in the concentration are more pronounced in the lower to middle troposphere (800 to 300 hPa, or 2 to 9 km altitude), but the absolute changes (up to 8 ppbv in June, see Figure 1 lowest panels) are largest at higher altitudes (between 300 and 200 hPa or 9 and 12 km) in the extratropics of the Northern Hemisphere. When examining the relative changes, we also note that the location of the maximum response evolves with latitude following the mean solar radiation. The largest response is most pronounced first in the tropics (March and April) with a gradual displacement towards the northern polar region (May to July).

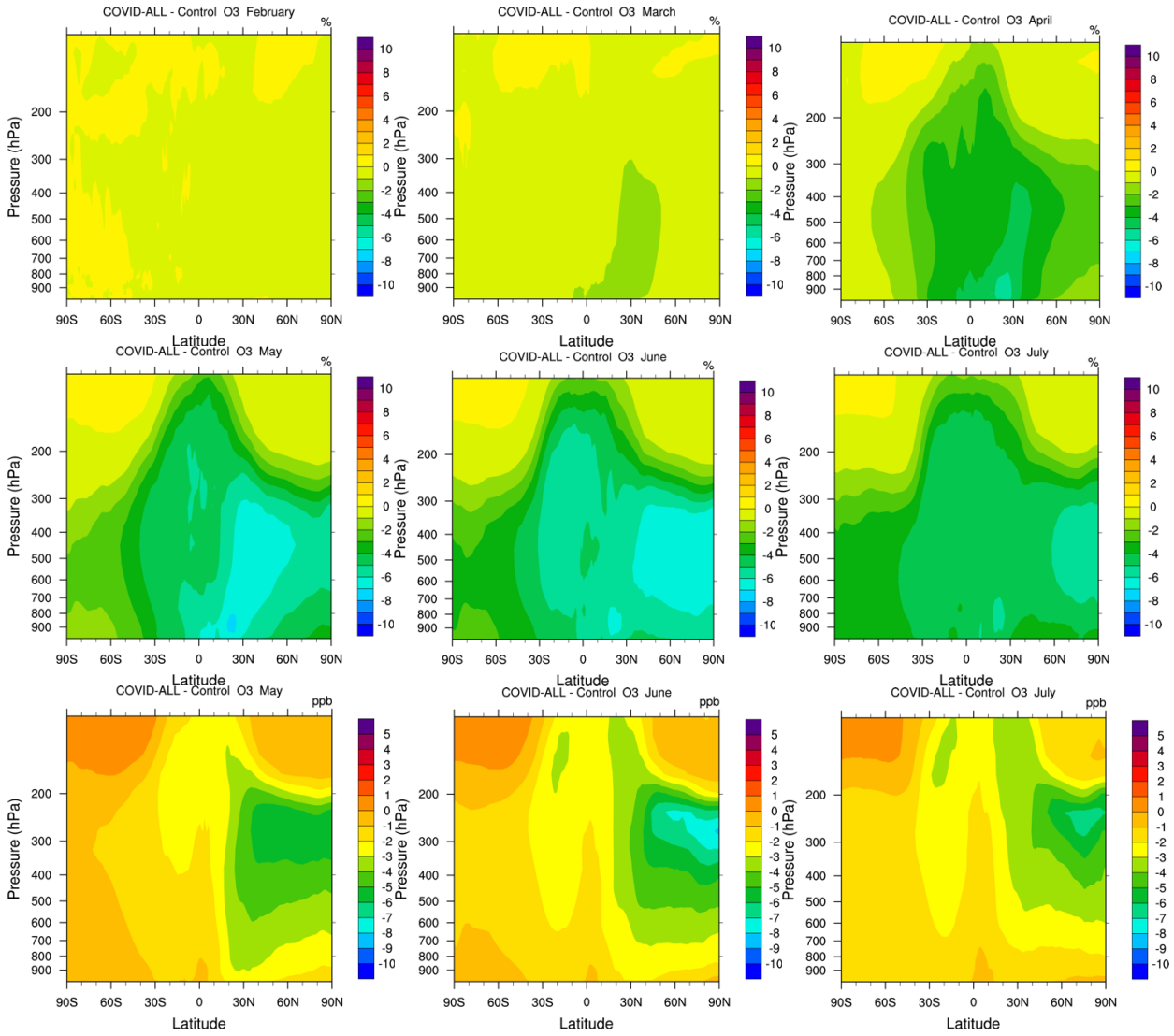

Figure 1. Change in the zonally and monthly averaged ozone mixing ratio between the surface and the upper troposphere for different months in response the combined changes in the emissions of pollutants during the COVID-19 pandemic (case 3). The two upper rows show relative changes from February to July 2020 (percent). The lowest row shows similar results but in absolute terms (ppbv) for the period May to July 2020.

We now investigate the contribution of the different forcing factors that explain the calculated ozone anomaly. We focus here on June 2020 during which the ozone reduction is largest. In Figure 2, we show the response of zonal and monthly mean concentrations of NO_x, ozone, hydroxyl (OH) and peroxy (HO_2) radicals and particulate matter to the changes in surface emissions (middle panels, case 1) and aircraft emissions (right panels, case 2), and to the combined changes (left panels, case 3). In the case of NO_x, the response to the reduced surface

emissions (case 1) is generally largest in the planetary boundary layer (larger than 10%), except in the tropics where NO_x-depleted near-surface air masses are lifted to the upper troposphere by convective transport resulting in 5 to 8 % reductions in the concentrations. The effect of tropical convection is also visible in the case of ozone (reduction of 3 - 4%) and $PM_{2.5}$ (reduction of 5 - 8%). The depleted tropical NO_x leads to a slower HO_2 to OH conversion, and explains the reduced OH (3 to 5 x 10^3 pptv or 3 to 4%) and the enhanced HO_2 concentrations (2 to 3%) near the equator.

Large concentration changes resulting from the dramatic reduction in air traffic during the pandemic (case 2) are derived by the model. Between 300 to 200 hPa (9 and 12 km), the zonal and monthly mean NO_x concentration is reduced by more than 20% north of 30°N, while that of ozone is reduced by 4 to 5% north of 60°N. Because of the increase with altitude of the background ozone concentration, the maximum ozone depletion in relative terms is located near 400 hPa (7 km), while in absolute terms (reduction of 7 ppbv), it is located higher in the atmosphere near 250 hPa (10 km). A secondary maximum decrease in the NO_x concentration of 7 % is found near 30°S. The reduced NO_x levels along the flight corridors tend to reduce the OH concentration by more than 1 x 10^{-2} pptv (about 10 %) between 400 and 200 hPa (about 7 to 12 km) at 45°N and between 400 and 300 hPa (7 and 9 km) in the polar Arctic region, and hence induce in these regions an increase in HO_2 levels of typically 40 x 10^{-2} pptv (20%). The small OH concentration increase of up to 0.6 x 10^{-2} pptv (3%) between 200 and 250 hPa in the polar region (concomitant with a HO_2 increase of 15-20%) is attributed to the enhanced penetration of solar radiation under high zenith angles associated with the slight reduction of ozone at these heights. The reduction in $PM_{2.5}$ associated with reduced air traffic reaches 15% near 300 hPa and results from a reduction of similar magnitude in the concentration of sulfate and black carbon particles.

The zonally averaged perturbations in June, resulting from the combined changes in surface and aircraft emissions during the pandemic relative to the baseline simulation (case 3), are shown by the left panels of Figure 2. In the specific case of NO_x, the relative reduction in the concentration is higher than 10% in the boundary layer at several latitudes and in the upper

troposphere north of 30°N and between 40°S to 15°S. In the case of ozone, the calculated reduction in June reaches 6 to 7 percent north of 30°N between 800 and 300 hPa (2 and 9 km). The reduction is close to 5% in the tropics (30°S to 30°N) and extends up to the tropopause. Results for SO_2, sulfate particles and black carbon (soot) are displayed in Figure S4. Vertical profiles of the changes in the monthly and zonally mean ozone reductions (in ppbv) relative to the baseline simulation and calculated poleward of 65°S in the tropics and poleward of 65°N are shown in Figure S5.

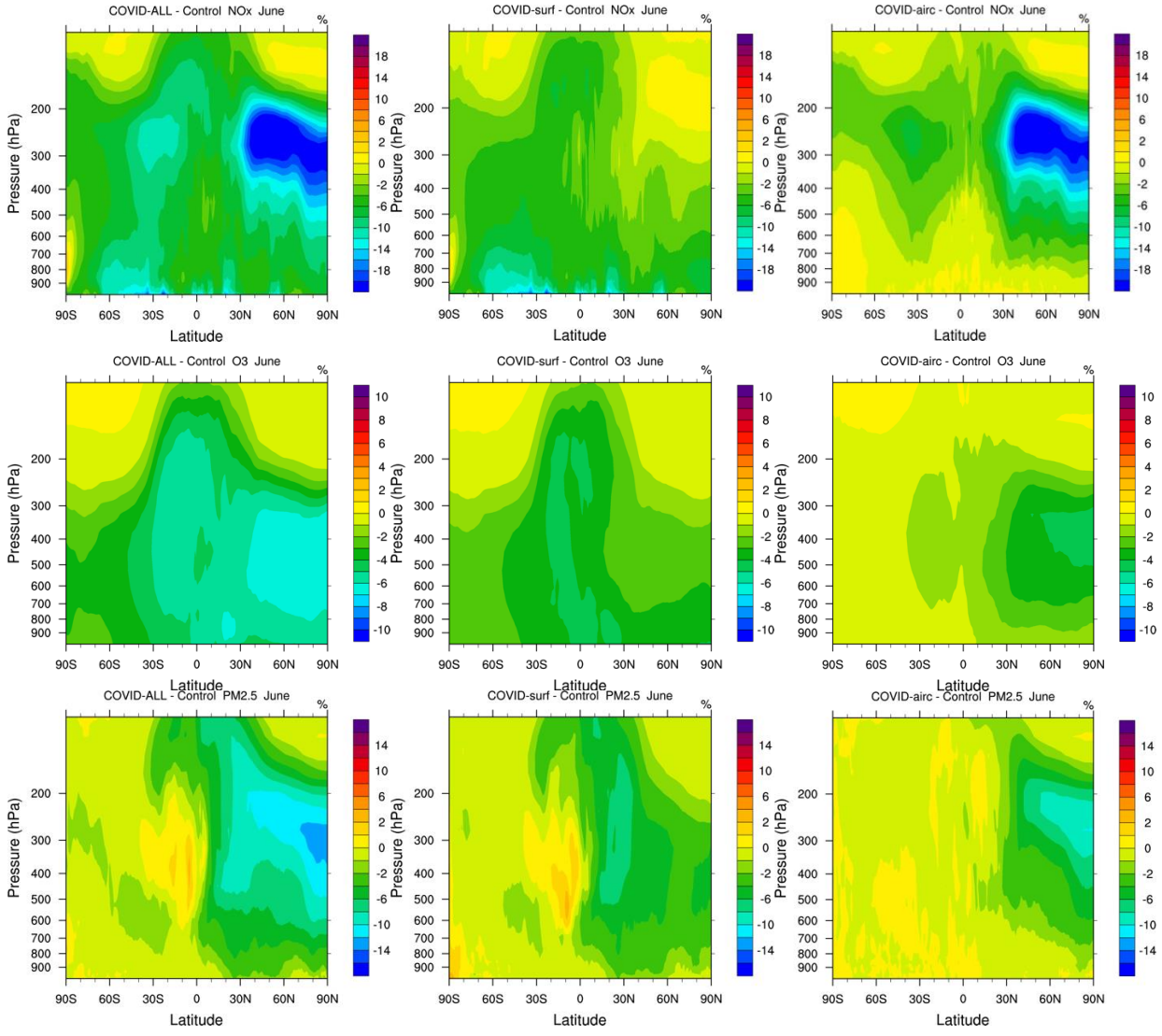

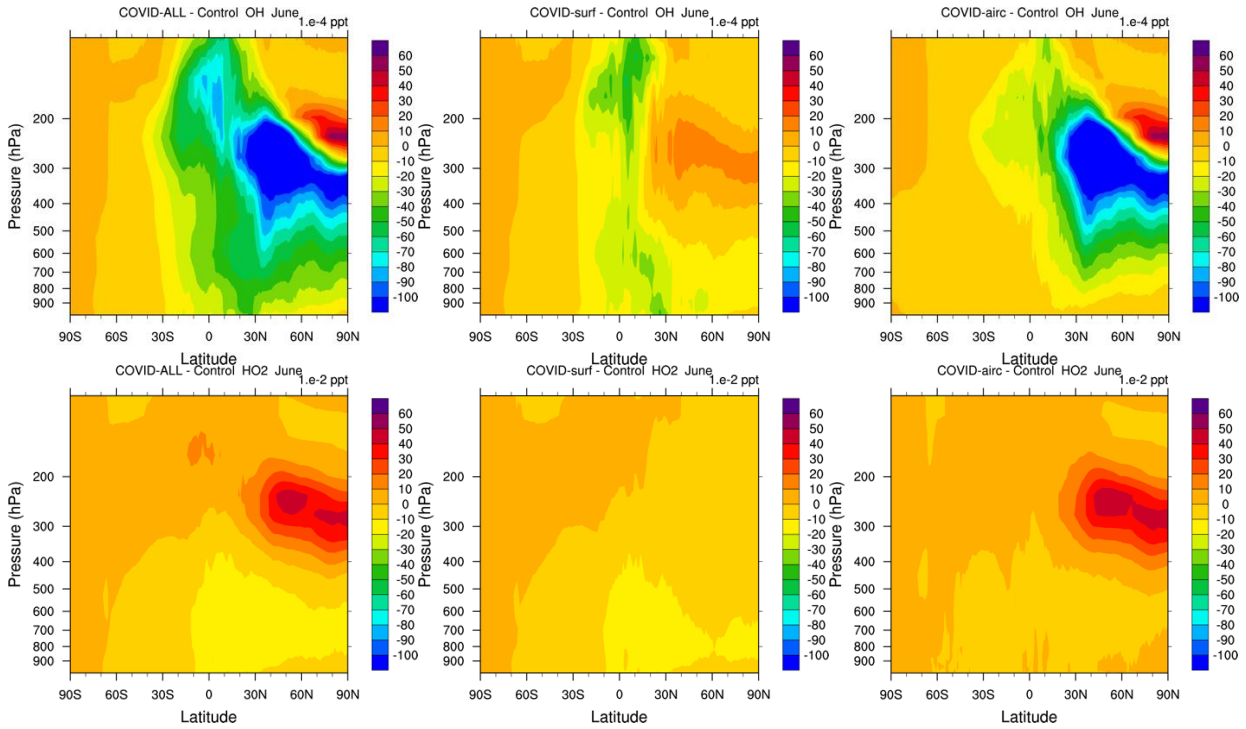

Figure 2. Change from the surface to the lower stratosphere in the zonally and monthly averaged concentration of NO_x (percent), ozone (percent), $PM_{2.5}$ (percent), OH (10^{-4} pptv) and HO_2 (10^{-2} pptv) in June 2020 relative to a baseline case in which the COVID-19 related changes in the emissions or primary species are ignored. Left: response to changes in surface and air traffic emissions (case 3); Middle: response to changes in surface emissions only (case 1); Right: response to the reduction in aircraft emissions (case 2).

In order to provide some insight into the longitudinal distribution of the perturbed chemical fields, we show in Figure S6 the anomaly in NO_x and ozone at the 273 hPa level (about 10 km), a layer of the atmosphere that is strongly affected by aircraft emissions. We see that the NO_x levels are considerably reduced over Europe (more than 30%) and over the Northern Atlantic Ocean as well as over the eastern and western US (between 10 and 25%) and the Pacific Ocean (up to 20–25%). Noticeable reductions are also found along the Brazilian coast (15%) and in eastern Australia (10- 15%). The small increases seen in the tropics result from enhanced NO_x emissions in the residential sector during the pandemic. The reduction in ozone at 273 hPa shown here for June 2020 is relatively uniformly distributed (5%) with the largest values found over Europe and the Northern Atlantic (7–8%).

4. Effects of 2020 meteorological conditions and comparison with observations

The interannual variations in the strength of the stratospheric circulation and dynamical variability impact the tropospheric ozone burden (Archibald et al., 2020). Specifically, deep intrusions of stratospheric ozone frequently reach the middle and even lower troposphere at midlatitudes during winter and spring, and can contribute significantly to ozone variability in the troposphere (Terao et al., 2008). This meteorologically induced variability (case 4) needs to be accounted for, e.g., when comparing our simulations with observed changes (case 5). Particularly in 2020, early and persistent cold conditions led to an exceptionally stable polar vortex and to record-low ozone in the Arctic, as highlighted by MLS observations (Manney et al., 2020), ozone sondes measurements (Wohltmann et al., 2020) and chemical reanalyses by the Copernicus Atmosphere Monitoring Service (CAMS, Inness et al., 2020). The minimum ozone column occurred in the first half of March, with March and April 2020 corresponding to the lowest ozone recorded for the period 1979 to 2020.

We show in the Supplementary Information (Figure S7) that the anomalies in monthly mean NO_x concentrations calculated in June 2020 relative to our adopted climatology and resulting from interannual variations in atmospheric circulation and temperature, lightning-related NO_x formation and wildfire-related emissions (case 4) are large, up to 25%, and comparable to the effect generated by the COVD-19 outbreak, up to -20% (case 3). Based on the "meteorological" model estimates (top left panel, case 4), NO_x should have been abnormally abundant in the free troposphere during 2020, particularly in the northern hemisphere. However, the perturbations in emissions due to the pandemic substantially reduced the NO_x level in northern hemisphere and tropics (top right Panel, case 5).

Poleward of 45°N, the anomaly in the zonally and monthly mean free tropospheric ozone concentration relative to the 19-year climatology is influenced substantially by the pronounced springtime Arctic ozone depletion in the first months of 2020 (case 4, bottom left panel of Figure S7). This anomaly persisted between 400 and 20 hPa, poleward of 60°N, as late as June, although with a considerably lower amplitude. The ozone concentration anomaly resulting from the perturbed emissions during the COVID-19 pandemic combined with the interannual variability ranges from 5 to 15 percent north of 30°N (case 5, bottom right panel of Figure S7).

Averaged vertical profiles of the anomalies are provided in Figures S8 (polar latitudes) and S9 (hemispheric and tropical averages).

It is interesting to note that meteorologically-induced positive ozone anomalies everywhere south of 30°N in 2020 (bottom left panel of Figure S7, case 4) appear to have masked the COVID-19 related ozone reductions in this region (see Figures 1 and 2, case 3). The net ozone anomaly in 2020 was therefore small south of 30°N (bottom right panel of Figure S7, case 5), which is consistent with the lack of large negative anomalies derived from the observations in the tropics and in the Southern Hemisphere (Steinbrecht et al. 2021, and Figs. S10, S12, S13).

For the northern hemisphere, the comparison between our simulations (case 5) and the observations of Steinbrecht et al., (2021) is shown in Figure 3. Ozone monthly means of the year 2020, at about 45 locations worldwide (see Figure S10 for a map of the locations), are compared against the 2000 to 2019 climatology. Figure 3 also shows results from the Copernicus Atmospheric Monitoring Service (CAMS), which do not include effects of the reduced emissions in 2020 (case 4). Panel a.) of Figure 3) shows the resulting annual courses of ozone anomalies at 6 kilometers altitude (~420 hPa), averaged over all northern extratropical stations (stations north of 15°N). All data sets show increasingly negative anomalies from January to April 2020, largely due to 2020 meteorological conditions and Arctic stratospheric ozone depletion in 2020 (compare Figure S7). Observations and CAMS show similar decline from January to April, our CAM-chem simulations (case 5) give less of a decline. From April onwards, photochemical ozone production becomes increasingly important, and the reduced emissions of 2020 play a major role (compare Figure 1 and S9). Consequently, observations and CAM-chem simulations show persistent negative anomalies (case 5) of -5 to -10%. Note the slight difference between the two CAM-chem simulations from May to August. The simulation with larger and more realistic Arctic stratospheric springtime ozone depletion following Wilka et al. (2021) (NCAR_W, thick light red line) gives about 1% more ozone reduction from May to August, and is generally in better agreement with the observations (thick blue lines, see also panels b.-d.)). In contrast to observations and both CAM-chem simulations (case 5), CAMS (case 4, grey lines) simulates increasing ozone from May onwards. By July, CAMS simulates anomalies near or above zero.

311 The good agreement between observations and CAM-chem simulations (case 5) from April to
312 August, and their difference with respect to CAMS (case 4), further confirms that the negative
313 ozone anomaly of -5 to -10% in late spring and summer 2020 was caused largely by reduced
314 emissions, with some influence from the 2020 Arctic spring-time depletion of stratospheric
315 ozone.

316

317 To complete the picture, panels b.- d. in Figure 3 show vertical profiles of the ozone anomaly,
318 averaged over the 4 months from April to August 2020, and for April and June. In all three
319 panels, good agreement and overlapping error bars are shown for observations and CAM-chem
320 simulations (case 5), whereas CAMS (case 4) shows 5 to 7% higher ozone at all levels up to 150
321 hPa, consistent with the simulated effect of reduced emissions in Figure 1.

322

323 Figures S11 to S13 in the supplement show similar comparisons for other latitude bands. For
324 high latitudes, north of 65°N (Figure S11), meteorological conditions of 2020 and the large
325 stratospheric springtime ozone depletion (case 4) are the major contributors to low ozone in
326 2020, certainly at levels above 500 hPa (see also Figure S7). The effects of the reduced
327 emissions are less pronounced, and appear mostly in summer below 500 hPa (~-5%), possibly
328 also around 200 hPa, -5 to -10% due to air-traffic reductions. In the tropics and Southern
329 Hemisphere (Figure S12, S13), observations, CAM-chem simulations, and CAMS show similar
330 meteorological ozone anomalies in 2020, with no indication of significant changes due to
331 emission reductions in 2020.

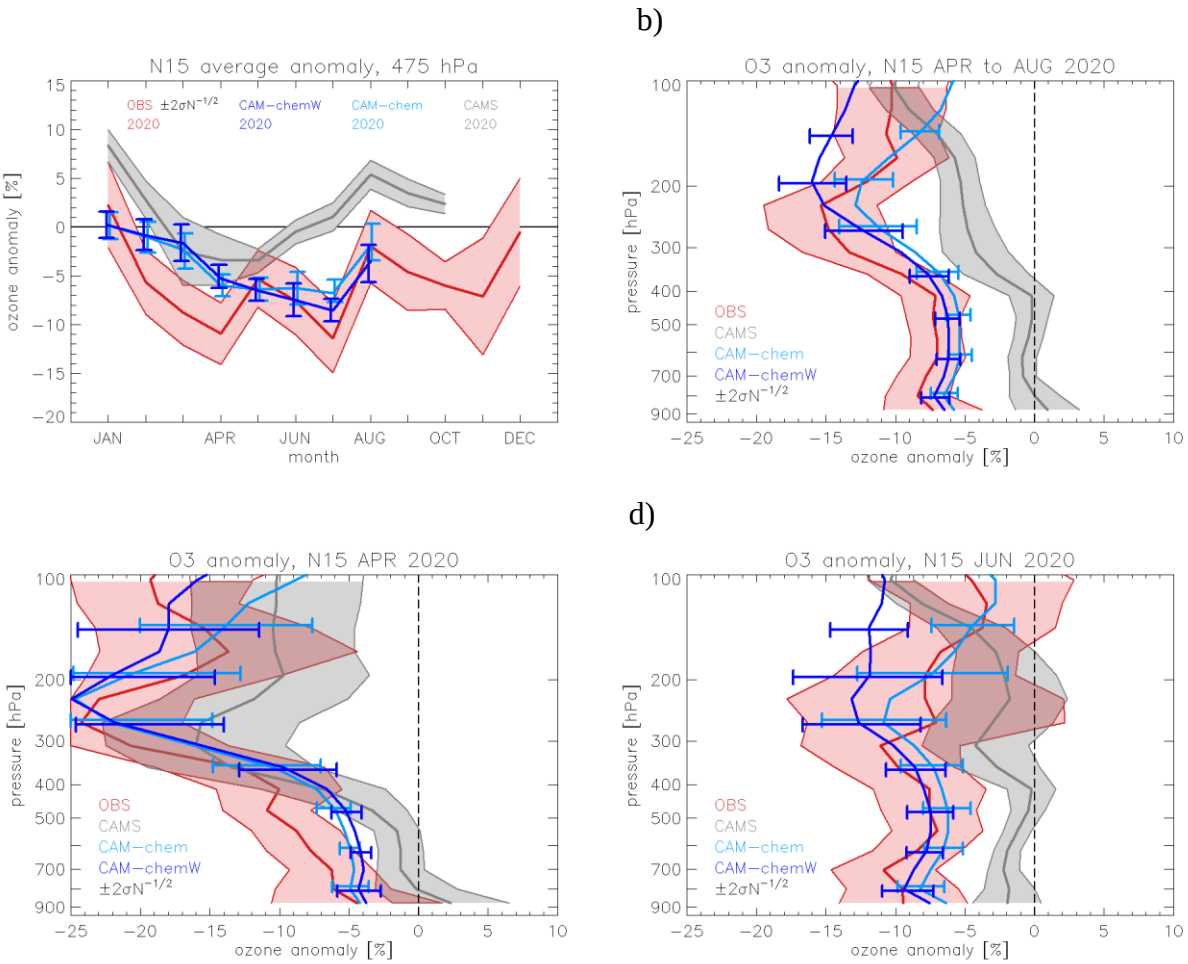

Figure 3. Panel a.) annual course of 2020 ozone anomalies at 6 km altitude (~420 hpa), averaged over stations north of 15°N, as in Steinbrecht et al. (2021). Red: observations (case 5). Light and dark blue: CAM-chem simulation (case 5), and CAM-chem simulation with more realistic Arctic stratospheric spring-time ozone depletion following Wilka et al. (2021). Grey: CAMS simulation (case 4). Panels b) to d): Profiles of the 2020 mean anomaly over stations north of 15°N for April to August, April, and June. Error bars (or shading) give ±2 standard deviations of the mean over stations.

5. Summary

The ozone abundance in the extratropical northern hemisphere free troposphere during the spring and summer of 2020 has been 5 to 15% lower than climatology. The response to the decreased emissions of primary pollutants associated with the reduction in economic activity including air-traffic during the COVID-19 pandemic is estimated to be 4 to 8%. Substantial changes are also found in the level of oxidants (OH and HO_2). Reduced worldwide aircraft operations had the highest impact in the middle and upper troposphere of the northern hemisphere during the

summer months. The impact of 2020 meteorological conditions and the abnormally high ozone depletion in the Arctic lower stratosphere during the spring and summer of 2020 produces a noticeable ozone reduction of 3 to 10 % in the northern extratropical free troposphere. This effect is noticeable until late spring and reaches a maximum in June. Below 400 hPa, the influence of the stratosphere remains small compared to the effect of the COVID-19-related reduction. For regions south of 30°N, the tropics and the southern hemisphere, the simulations indicate that a 4 to 6% reduction of ozone due to COVID-19 related emission reductions did take place in 2020, but was largely compensated by ozone (and nitrogen oxides) increases caused by the specific meteorological conditions of 2020.

Finally, our study investigates the response of free tropospheric ozone to an unprecedented real case reduction in global anthropogenic emissions. The model simulations successfully reproduce the observed ozone anomalies in the free troposphere during the six months that followed the COVID-19 outbreak. Further, they provide a quantitative estimate of the different factors that contributed to the observed ozone anomalies. Clearly, global and regional air quality forecast and reanalysis models must account for the disturbances that occurred in the atmospheric chemical system after January 2020.

Data availability

CESM2.2.0 is a publicly released version of the Community Earth System Model and freely available online (at www.cesm.ucar.edu, last access: 2 October 2020). The results of the model simulations are available online (Gaubert et al., 2021, https://doi.org/10.5065/cgg0-rr19). The CAMS-GLOB-ANT_V4.2_R1.1 surface emissions and the CONFORM adjustment factors are publicly available from the ECCAD database (eccad.aeris-data.fr).

Acknowledgments

We would like to acknowledge the high-performance computing support from Cheyenne (doi:10.5065/D6RX99HX) provided by NCAR's Computational and Information Systems Laboratory of the National Center for Atmospheric Research (NCAR), sponsored by the US National Science Foundation (NSF). This material is based upon work supported by the National Center for Atmospheric Research, which is a major facility sponsored by the National Science Foundation under cooperative agreement no. 1852977. We also acknowledge the support of the AQ-WATCH European project, a HORIZON 2020 Research and Innovation Action (GA 870301). The surface emissions adopted in the present study are based on the CAMS-GLOB-ANT dataset that has been developed with the support of the CAMS (Copernicus Atmosphere Monitoring Service), operated by the European Centre for Medium-Range Weather Forecasts on behalf of the European Commission as part of the Copernicus Programme. T. W. and Y. L. acknowledge support by the Hong Kong Research Grants Council (T24-

504/17-N and A-PolyU502/16). T.S. acknowledges the support of the ICOVAC and TROVA projects funded by ESA.

Author contributions:

Conceptualization: Guy Brasseur, Benjamin Gaubert, Idir Bouarar, Wolfgang Steinbrecht
Production of emissions: Sabine Darras, Thierno Doumbia, Claire Granier, Nellie Elguindi
Analysis observations: Wolgang Steinbrecht
Model simulations: Benjamin Gaubert, Simone Tilmes
Analysis of the model results: Guy Brasseur, Idir Bouarar, Benjamin Gaubert, Trissevgeni Stavrakou, Jean-François Müller, Tao Wang, Adrien Deroubaix, Forrest Lacey, Xiaoqin Shi.
Writing -original draft: Guy Brasseur, Wolfgang Steinbrecht, Benjamin Gaubert
Writing -review and editing: All authors.

References

Archibald, A. T., et al. 2020. Tropospheric Ozone Assessment Report: A critical review of changes in the tropospheric ozone burden and budget from 1850 to 2100. *Elementa, Science of the Anthropocene, 8*: 1., https://doi.org/10.1525/elementa.2020.034.

Bates, K. H. and Jacob, D. J. (2020). An Expanded Definition of the Odd Oxygen Family for Tropospheric Ozone Budgets: Implications for Ozone Lifetime and Stratospheric Influence, *Geophysical Research Letters, 47*(4) https://doi.org/10.1029/2019GL084486.

Bauwens, M., Compernolle, S., Stavrakou, T., Müller, J.-F., van Gent, J., Eskes, H., … Zehner, C. (2020). Impact of coronavirus outbreak on NO_2 pollution assessed using TROPOMI and OMI observations. *Geophysical Research Letters*, *47*, e2020GL087978. https://doi.org/10.1029/2020GL087978.

Cazorla, M., Herrera, E., Palomeque, E., Saud, N. (2020). What the COVID-19 lockdown revealed about photochemistry and ozone production in Quito, Ecuador, *Atmospheric Pollution Research*, in press., https://doi.org/10.1016/j.apr.2020.08.028.

Danabasoglu, G., Lamarque, J.-F., Bacmeister, J., Bailey, D. A., DuVivier, A. K., Edwards, J., et al. (2020). The Community Earth System Model Version 2 (CESM2). *Journal of Advances in Modeling Earth Systems*, 12, e2019MS001916. https://doi.org/10.1029/2019MS001916.

Doumbia, T., Granier, C., Elguindi, N., Bouarar, I., Darras, S., Brasseur, G., Gaubert, B., Liu, Y., Shi, X., Stavrakou, T., Tilmes, S., Lacey, F., Deroubaix, A., and Wang, T. (2021). Changes in global air pollutant emissions during the COVID-19 pandemic: a dataset for atmospheric chemistry modeling, *Earth System Science Data Discussion*. [preprint], https://doi.org/10.5194/essd-2020-348, in review.

Elguindi, N., Granier, C., Stavrakou, T., Darras, S., Bauwens, M., Cao, H., C. Chen, H.A.C. Denier van der Gon, O. Dubovik, T.M. Fu, D.K. Henze, Z. Jiang, S. Keita, J.J.P. Kuenen, J. Kurokawa, C. Liousse, J.F. Muller, Z. Qu, F. Solmon, B. Zheng (2020). Intercomparison of magnitudes and trends in anthropogenic surface emissions from bottom-up inventories, top-down estimates, and emission scenarios, *Earth's Future, 8*, e2020EF001520. doi:10.1029/2020EF001520.

Emmons, L. K., Schwantes, R. H., Orlando, J. J., Tyndall, G., Kinnison, D., Lamarque, J.-F., … Pétron, G. (2020). The Chemistry Mechanism in the Community Earth System Model version 2 (CESM2).

Journal of Advances in Modeling Earth Systems, *12*, e2019MS001882. https://doi.org/10.1029/2019MS001882.

Gaubert, B., Emmons, L.K., Reader, K., Tilmes, S., Miyazaki, K., ... Ren, X. (2020). Correcting model biases of CO in East Asia: impact on oxidant distributions during KORUS-AQ. *Atmospheric Chemistry and Physics 20*, 14617–14647, https://doi.org/10.5194/acp-20-14617-2020, 2020.

Gaubert, B., Bouarar, I., Doumbia, T., Liu, Y., Stavrakou, T., Deroubaix, A., Darras, S., Elguindi, N., Granier, C., Lacey, F., Müller, J.-F., Shi, X., Tilmes, S., Wang, T. and Brasseur G. P. (2021). Global Changes in Secondary Atmospheric Pollutants during the 2020 COVID-19 Pandemic, *Journal of Geophysical Research*, in press, doi/10.1002/essoar.10504703.1

Gaubert, Benjamin, Tilmes, Simone, Bouarar, Idir, Doumbia, Thierno, Liu, Yiming, Stavrakou, Trissevgeni, Deroubaix, Adrien, Darras, Sabine, Elguindi, Nellie, Granier Forrest Lacey, Claire, Müller, Jean-François, Shi, Xiaoqin, Wang, Tao, Brasseur, Guy. (2020). CAM-chem simulation of the 2020 lockdown. Version 3.0. UCAR/NCAR - DASH Repository. https://doi.org/10.5065/cgg0-rr19. Accessed 09 Mar 2021.

Gelaro, R., McCarty, W., Suarez, M.J., … B. Zhao (2017) The Modern-Era Retrospective Analysis for Research and Applications, Version 2 (MERRA-2), *Journal of Climate, 30*(14), 5419-5454 https://doi.org/10.1175/JCLI-D-16-0758.1.

Gettelman, A., Mills, M. J., Kinnison, D. E., Garcia, R. R., Smith, A. K., Marsh, D. R., … Randel, W.J. (2019). The whole atmosphere community climate model version 6 (WACCM6). *Journal of Geophysical Research: Atmospheres, 124*, https://doi.org/10.1029/2019JD030943.

Goldberg, D. L., Vinciguerra, T. P., Hosley, K. M., Loughner, C. P., Canty, T. P., Salawitch, R., and Dickerson, R. R. (2015). Evidence for an increase in the ozone photochemical lifetime in the eastern United States using a regional air quality model, *Journal of Geophysical Research 120*(24), 12778-12793, https://doi.org/10.1002/2015JD023930.

Granier, C., S. Darras, H. Denier van der Gon, J. Doubalova, N. Elguindi, B. Galle, M. Gauss, M. Guevara, J.-P. Jalkanen, J. Kuenen, C. Liousse, B. Quack, D. Simpson, K. Sindelarova (2019). The Copernicus Atmosphere Monitoring Service global and regional emissions, *Copernicus Atmosphere Monitoring Service* (CAMS) report, doi:10.24380/d0bn-kx16.

Huang, X., Ding, A., Gao, J., Zheng, B., Zhou, D., Qi, X., … He, K. (2020) Enhanced secondary pollution offset reduction of primary emissions during COVID-19 lockdown in China, *National Science Review*, https://doi.org/10.1093/nsr/nwaa137.

Hoesly, R. M., Smith, S. J., Feng, L., Klimont, Z., Janssens-Maenhout, G., Pitkanen, T., Seibert, J. J., Vu, L., Andres, R. J., Bolt, R. M., Bond, T. C., Dawidowski, L., Kholod, N., Kurokawa, J.-I., Li, M., Liu, L., Lu, Z., Moura, M. C. P., O'Rourke, P. R., and Zhang, Q. (2018) Historical (1750–2014) anthropogenic emissions of reactive gases and aerosols from the Community Emissions Data System (CEDS), *Geosciences Model Development, 11*, 369–408, https://doi.org/10.5194/gmd-11-369-2018.

Inness, A., Chabrillat, S., Flemming, J., Huijnen, V., Langenrock, B., Nicolas, J., et al. (2020). Exceptionally low Arctic stratospheric ozone in spring 2020 as seen in the CAMS reanalysis. *Journal of Geophysical Research: Atmospheres, 125*, e2020JD033563. https://doi.org/10.1029/2020JD033563.

Lawrence, D. M., Fisher, R. A., Koven, C. D., Oleson, K. W., Swenson, S. C., Bonan, G., et al. (2019). The Community Land Model version 5: Description of new features, benchmarking, and impact of forcing uncertainty. *Journal of Advances in Modeling Earth Systems, 11*, 4245–4287. https://doi.org/10.1029/2018MS001583

Le, T., Wang, Y., Liu, L., Yang, J., Yung, Y. L., Li, G., and Seinfled, J. H. (2020). Unexpected air pollution with marked emission reduction during the COVID-19 outbreak in China, *Science, 369*, 702-706, doi: 10.1126/science.abb7431

Lian, X., Huang, J., Huang, R., Liu, C., Wang, L. & Zhang, T. (2020). Impact of city lockdown on the air quality of COVID-19-hit of Wuhan city. *Science of the Total Environment, 742*, 140556, https://doi.org/10.1016/j.scitotenv.2020.140556.

Liu, X., Ma, P.-L., Wang, H., Tilmes, S., Singh, B., Easter, R. C., Ghan, S. J., & Rasch P.J. (2016). Description and evaluation of a new four-mode version of the Modal Aerosol Module (MAM4) within version 5.3 of the Community Atmosphere Model. *Geoscientific Model Development*, *9* (2), 505–522. https://doi.org/10.5194/gmd-9-505-2016.

Liu, Y., Wang, T. Stravrakou, T., Elguindi, N., Doumbia, T., Granier, C., Bouarar, I., Gaubert B., and Brasseur G. P. (2020). Diverse response of atmospheric ozone to COVID-19 lockdown in China, *arXiv* preprint arXiv:2008:10851, https://arxiv.org/abs/2008.10851.

Manney, G. L., Livesey, N. J., Santee, M. L., Froidevaux, L., Lambert, A., & Lawrence, Z. D., et al. (2020). Record- low Arctic stratospheric ozone in 2020: MLS observations of chemical processes and comparisons with previous extreme winters. *Geophysical Research Letters, 47*, e2020GL089063. https://doi.org/10.1029/2020GL089063.

Mills, M. J., Schmidt, A., Easter, R., Solomon, S., Kinnison, D. E., Ghan, S. J., … Gettelman, A. (2016). Global volcanic aerosol properties derived from emissions, 1990–2014, using CESM1 (WACCM), *Journal of Geophysical Research: Atmospheres*, *121*, 2332–2348. https://doi.org/10.1002/2015JD024290.

Miyazaki, K., Bowman, K., Sekiya, T., Jiang, Z., Chen, X., Eskes, H., et al. (2020). Air quality response in China linked to the 2019 novel coronavirus (COVID-19) lockdown. *Geophysical Research Letters*, 47, e2020GL089252. https://doi.org/10.1029/2020GL089252.

Ordóñez, C., Garrido-Perez, J. M., García-Herrera, R. (2020). Early spring near-surface ozone in Europe during the COVID-19 shutdown: Meteorological effects outweigh emission changes, *Science of The Total Environment*, *747*, 141322, https://doi.org/10.1016/j.scitotenv.2020.141322

Shi, X., & Brasseur, G. P. (2020). The Response in Air Quality to the Reduction of Chinese Economic Activities during the COVID-19 Outbreak. *Geophysical Research Letters*, *47*, e2020GL088070. https://doi.org/10.1029/2020GL088070.

Steinbrecht, W., Kubistin, D., Plass-Dülmer, Davies, J., Tarasick, D.W., Gathen, P. et al. (2021). COVID-19 crisis reduces free tropospheric ozone across the Northern Hemisphere *Geophysical Research Letters*, 48, e2020GL091987. https://doi.org/10.1029/2020GL091987 .

Stevenson, D. S., et al. (2006). Multimodel ensemble simulations of present-day and near-future tropospheric ozone, *Journal of Geophysical Research*, *111*, D08301, doi:10.1029/2005JD006338.

Terao, Y., Logan, J. A., Douglass, A. R., and Stolarski, R. S. (2008), Contribution of stratospheric ozone to the interannual variability of tropospheric ozone in the northern extratropics, *Journal of Geophysical Research, 113*, D18309, doi:10.1029/2008JD009854.

Tilmes, S., Hodzic, A., Emmons, L. K., Mills, M. J., Gettelman, A., Kinnison, D. E., … Liu, X., (2020). Climate forcing and trends of organic aerosols in the Community Earth System Model (CESM2). *Journal of Advances in Modeling Earth Systems, 11,* 4323–4351. https://doi.org/10.1029/2019MS001827.

Venter, Z. S., Aunan, K., Chowdhury, S., and Lelieveld, J. (2020). COVID-19 lockdowns cause global air pollution declines, *Proceedings of the National Academy of Sciences, 117* (32) 18984-18990; DOI: 10.1073/pnas.2006853117.

Weber, J., Shin, Y. M., Staunton Sykes, J., Archer-Nicholls, S., Abraham, N. L., & Archibald, A. T. (2020). Minimal climate impacts from short-lived climate forcers following emission reductions related to the COVID-19 pandemic. *Geophysical Research Letters*, 47, e2020GL090326. https://doi.org/ 10.1029/2020GL090326

Wilka, C., Solomon, S., Kinnison, D., and Tarasick, D. (2021). An Arctic Ozone Hole in 2020 If not for the Montreal Protocol, *Atmospheric Chemistry and Physics Discussion,* https://doi.org/10.5194/acp-2020-1297.

Wohltmann, I., von der Gathen, P., Lehmann, R., Maturilli, M., Deckelmann, H., Manney, G. L., et al. (2020). Near-complete local reduction of Arctic stratospheric ozone by severe chemical loss in spring 2020. *Geophysical Research Letters, 47*, e2020GL089547. https://doi.org/ 10.1029/2020GL089547.

Supporting Information for

Ozone Anomalies in the Free Troposphere during the COVID-19 Pandemics

Idir Bouarar[1], Benjamin Gaubert[2], Guy P. Brasseur[1,2,9], Wolfgang Steinbrecht[3], Thierno Doumbia[4], Simone Tilmes[2], Yiming Liu[6], Trissevgeni Stavrakou[7], Adrien Deroubaix[1], Sabine Darras[4], Claire Granier[4,8], Forrest Lacey[2], Jean-François Müller[7], Xiaoqin Shi[1], Nellie Elguindi[4] and Tao Wang[9]

[1]Environmental Modeling Group, Max Planck Institute for Meteorology, Hamburg, Germany, [2]Atmospheric Chemistry Observations and Modeling Laboratory, National Center for Atmospheric Research, Boulder, CO, [3]Deutscher Wetterdienst, Hohenpeißenberg, Germany, [4]Laboratoire d'Aérologie, Université de Toulouse, CNRS, UPS, France, [5]Observatoire, Midi-Pyrénées, Toulouse, France, [6]School of Atmospheric Science, Sun Yat-sen University, Guangzhou, China, [7]Royal Belgian Institute for Space Aeronomy, Brussels, Belgium, [8]NOAA Chemical Sciences Laboratory/CIRES, University of Colorado, Boulder, CO. [9]Department of Civil and Environmental Engineering, The Hong Kong Polytechnic University, Hong Kong China,

Corresponding author: Guy P. Brasseur (guy.brasseur@mpimet.mpg.de)

Overview

We present here supplementary information that complements the presentation in the paper.

Table S1. Description of the Model Simulations

Simulation	Name	Description	Details
Sim. 1	CONTROL 2020	Baseline case for 2020.	2020 daily emissions with no COVID effects and with 2020 meteorology.
Sim. 2	COVID-surf	Effect of adjustments in 2020 surface emissions.	Same as Sim. 1, but with surface emissions adjusted for COVID effects
Sim. 3	COVID-airc	Effect of adjustments in 2020 aircraft emissions.	Same as Sim. 1, but with aircraft emissions adjusted for COVID effects
Sim. 4	COVID-ALL or COVID	Effects of combined adjustments in 2020 surface and aircraft emissions	Same as Sim. 1, but with surface and aircraft emissions adjusted for COVID effects
Sim. 5	CLIMO	2001-2019 simulation with emission trends accounted for	Mean seasonal evolution of chemical species derived by averaging the output over the period 2001-2019
Sim. 6	WACCM	Same as COVID-ALL	Nitric acid trihydrate (NAT) particle number density controlling denitrification of 10^{-5} particles cm^{-3}.

Table S2. Description of the Model Cases

Case		Differences between simulations	Description of the cases
1	COVID-surf minus CONTROL 2020	Sim. 2 – Sim. 1	Impact of adjustments in surface emissions during COVID
2	COVID-airc minus CONTROL 2020	Sim. 3 – Sim. 1	Impact of adjustments in aircraft emissions during COVID
3	COVID-all minus CONTROL 2020	Sim. 4 – Sim. 1	Impact of combined adjustments in surface and aircraft emissions during COVID
4	CONTROL 2020 minus CLIMO	Sim. 1 – Sim. 5	Change in the concentrations of chemical species with no COVID effects in 2020 relative to the 2001-2019 climatology
5	COVID-All minus EMIS-CLIMO	Sim. 4 – Sim. 5	Change in the concentrations of chemical species resulting from the adjusted emissions (surface and aircraft) relative to the 2001-2019 climatology

Text S1. Model description and baseline distribution of NO_x and ozone

Figure S1 shows the zonal and monthly mean mixing ratio (ppbv) of background NO_x and ozone during the months of April and June. We note the larger NO_x and ozone concentrations in the northern hemisphere. NO_x levels are highest in the boundary layers where the influence of surface emissions is largest as well as in the stratosphere where NO_x is produced by the oxidation of nitrous oxide. In the case of ozone, the mean surface mixing ratio is close to 20-25 ppbv (April) 25-30 ppbv (June) in the southern hemisphere and reaches 45-55 ppbv (April) and 35-40 ppbv (June) at 40^0N.

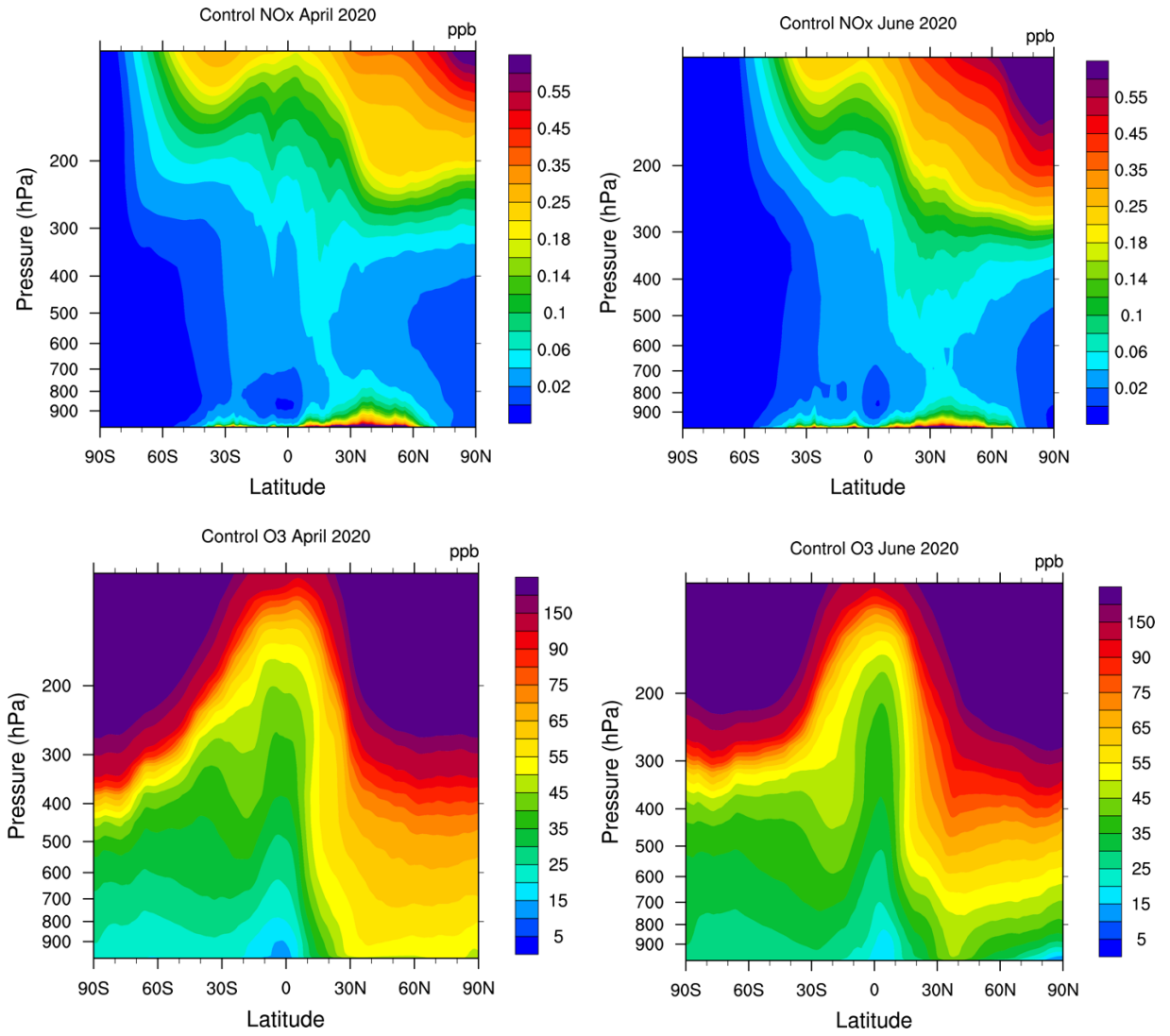

Figure S1. Zonally and monthly averaged NO_x and ozone mixing ratio for the months of April (left panels) and June 2020 (right panels) in the baseline case (control run) with no disturbance in the emissions associated with the COVID-19 outbreak.

Text S2. Adjustments of emissions during the COVID-19 pandemic (first wave)

The anthropogenic emissions are specified at a spatial resolution of 0.1 x 0.1 degree according to the CAMS-GLOB-ANT_v4.2-R1.1 global inventory (Granier et al., 2019, Elguindi et al., 2020). This inventory provides monthly-averaged emissions of the main chemical compounds and 25 speciated volatile organic compounds for the 2000-2020 period. To account for the effect of the COVID pandemic in 2020, the emissions of nitrogen oxides (NO_x), carbon monoxide (CO), volatile organic compounds (VOCs), sulfur dioxide (SO_2), black carbon (BC) and primary organic aerosols and SOA precursors (SVOC and IVOC) are modified by applying daily adjustment factors as provided in the CONFORM dataset developed by Doumbia et al. (2021). These factors for each economic sector (industrial, mobility, residential, energy) and

geographical region cover the period January to August 2020 (Figure S1) and are gridded at a spatial resolution of 0.1 x 0.1 degree (about 10 km x 10 km). We see that the largest changes in emissions took place first in China (January to March) and later in the other parts of the world (March to May). The reduction in the emissions by air traffic was most pronounced between April and June (about 80%).

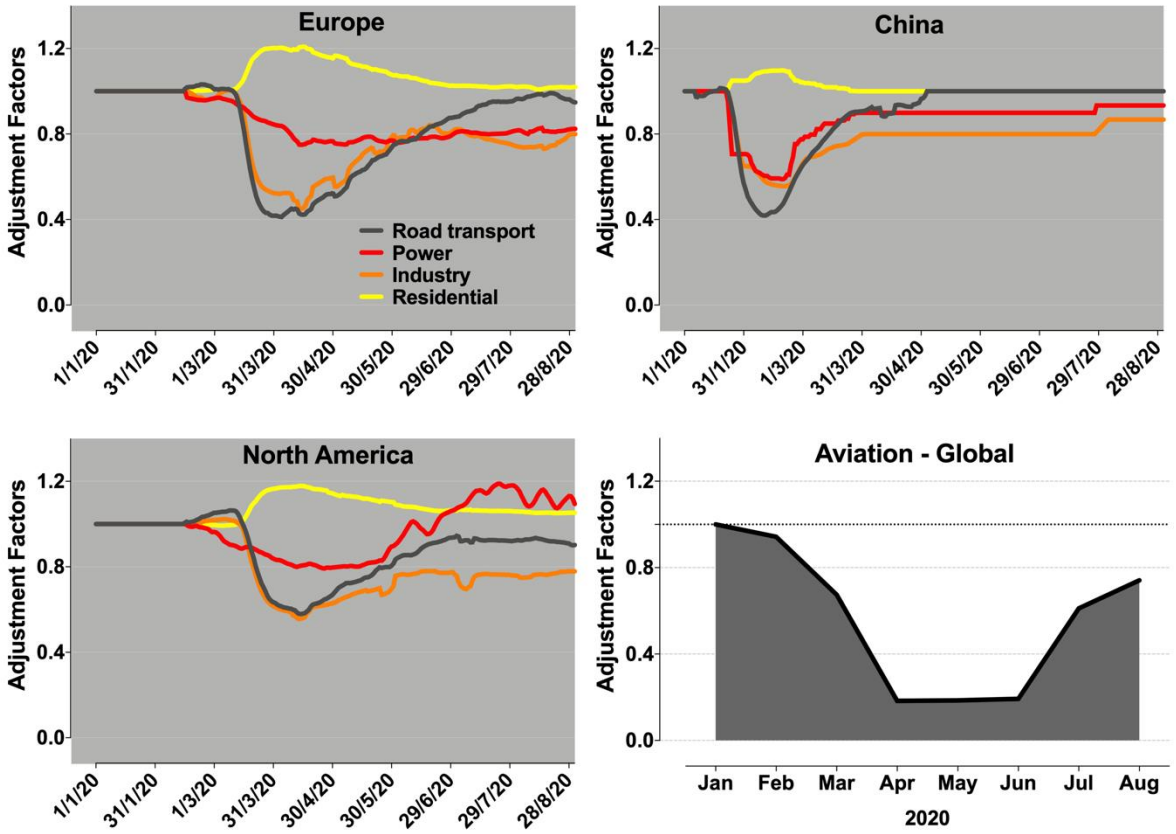

Figure S2. Adjustment factors applied in Europe, China and North America to the base surface emissions of chemical species (NO_x, CO, VOCs, SO_2) to account for the changes in economic activities (road transportation, power generation, industrial and residential activities) during the COVID-19 pandemic. The reduction in the global emissions resulting from the slowdown of air traffic is also shown.

Text S3

We report here the monthly mean changes in surface NO_x and ozone in response to changed emissions of primary pollutants during the COVID-19 pandemic. The results are shown for February, April and June 2020 and are expressed relative to a model simulation with identical meteorology but with standard emissions (no COVID-19 effect). We note the large reduction in surface NO_x concentration in China during February and the related change in surface ozone (increase in concentration in the northern part of the country and decrease in the southern regions). In the following months, the NO_x decrease spread in most regions of the world and ozone concentrations usually decrease, except in limited areas (large urban centers) where ozone is NO_x limited. See Gaubert et al, 2021 for a more detailed discussion.

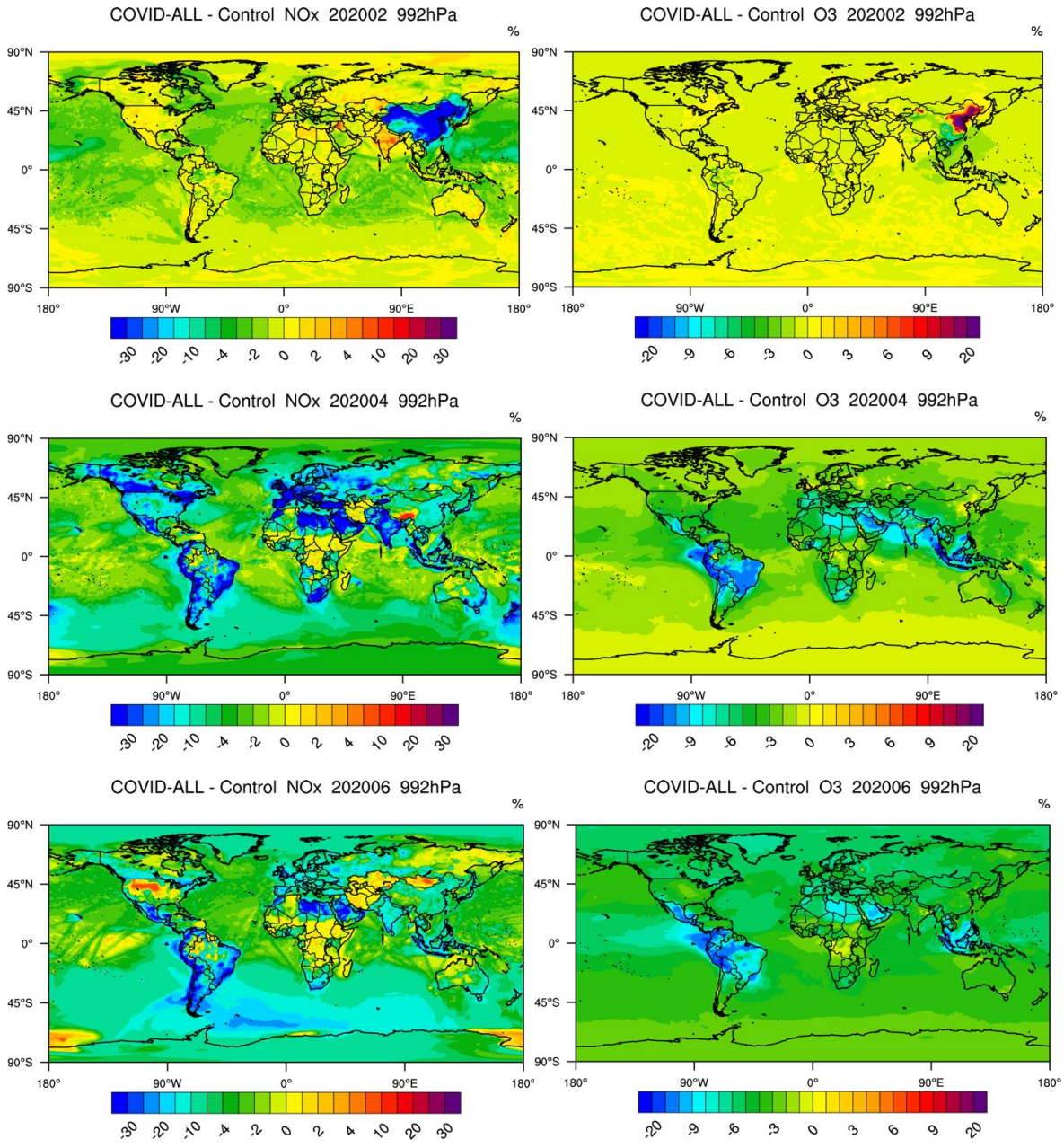

Figure S3. Global distribution of the percentage change in the NO_x (left) and ozone (right) concentrations near the surface during the COVID-19 pandemic (case 3). Top Panels: February 2020, Middle Panel: April 2020 and Lower Panel: June 2020.

Text S4.

Figure S4 presents results similar to those shown in Figure 2, but for other chemical species.

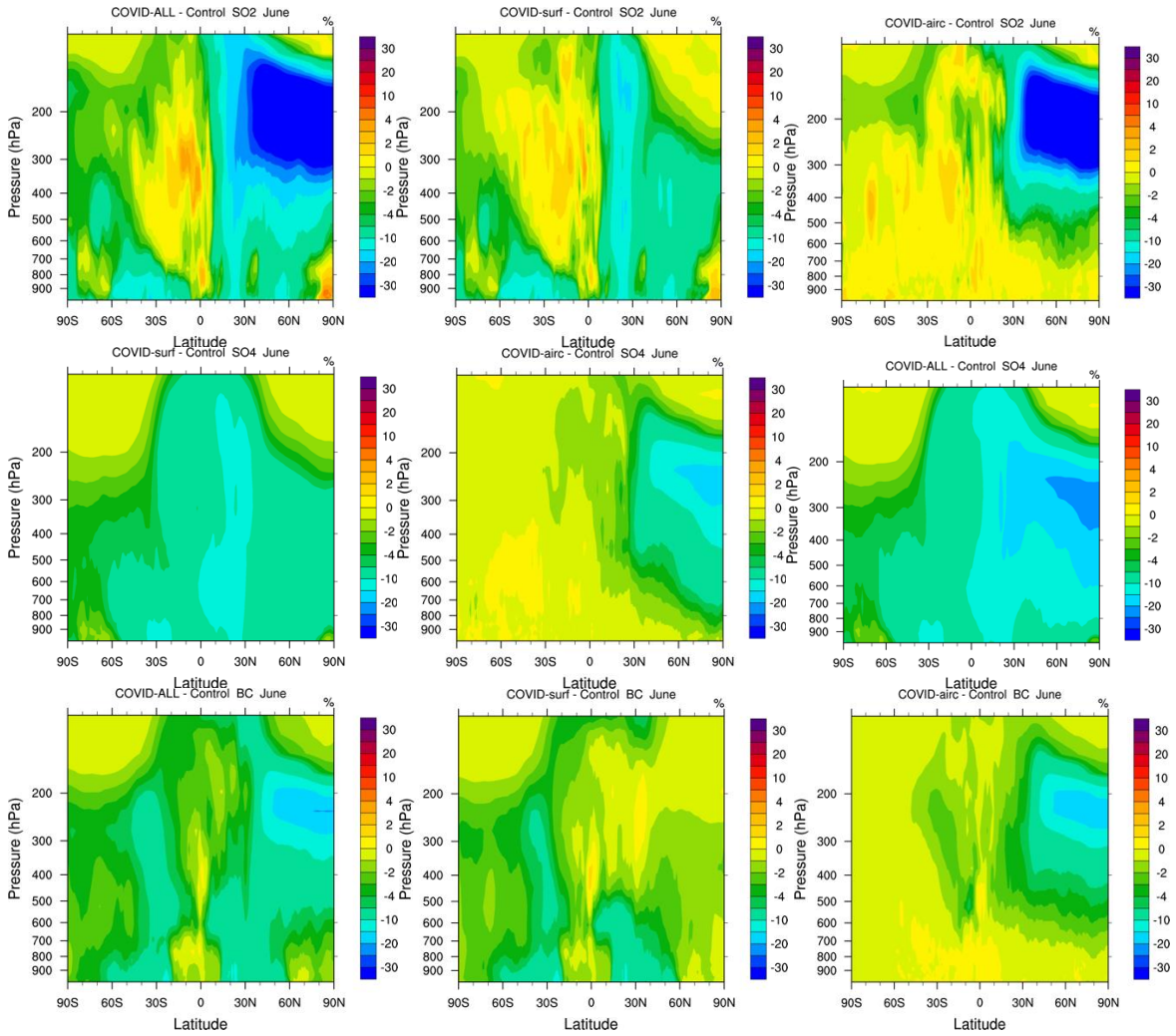

Figure S4. Change (percent) from the surface to the lower stratosphere in the zonally and monthly averaged concentration of SO_2, SO_4 and black carbon in June 2020 relative to a baseline case in which the COVID-19-related changes in the emissions of primary species are ignored. Left Panel: response to changes in surface and air traffic emissions (case 3); Middle Panel: response to changes in surface emissions only (case 1); Right Panel: response to the reduction in aircraft emissions (case 2).

Text S5.

We show in Figure S5 the relative change in the ozone concentration due to the change in surface emissions (red curves), to the reduction in air-traffic (green curves) and to the combined effects (blue curves). The meteorology in the baseline and perturbed cases is identical. The

calculated reduction at high latitudes varies with altitude from 1 to 7.5 percent in the northern hemisphere and from 0.7 to 1.3 percent in the southern hemisphere. In the tropics, the ozone reduction ranges from 1.0 to 3.5 percent. Figure S8 shows high latitude ozone responses when the meteorological variability is taken into account.

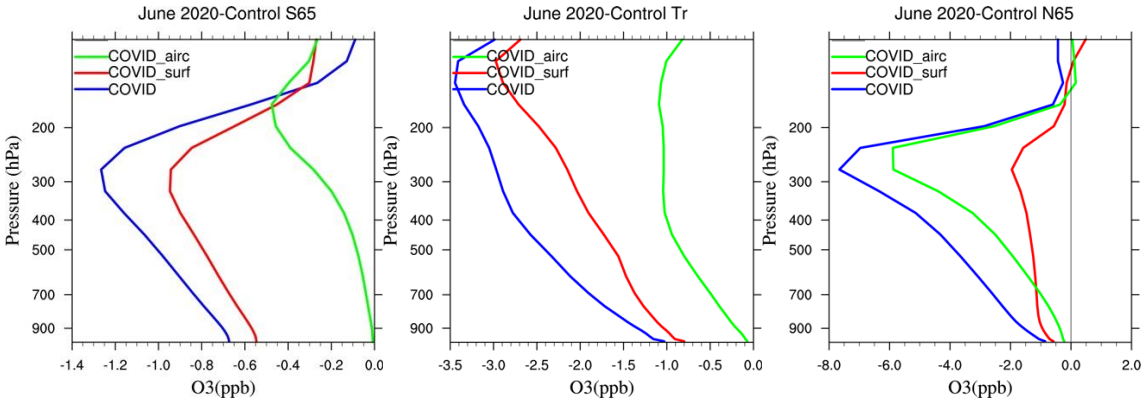

Figure S5. Vertical distribution of the changes (ppbv) in June 2020 monthly mean ozone concentration poleward of 65^0S (left panel), in the tropics (middle panel) and poleward of 65^0N (right panel) due to COVID-related changes in surface (red curves, case 1) and aircraft emissions (green curves, case 2). The two combined effects (case 3) are shown by the blue curves.

Text S6.

We show in Figure S6 the anomaly in NO_x and ozone at the 273 hPa level (about 10 km). The effect of the reduction in air traffic during the COVID-19 outbreak is dominant at this altitude.

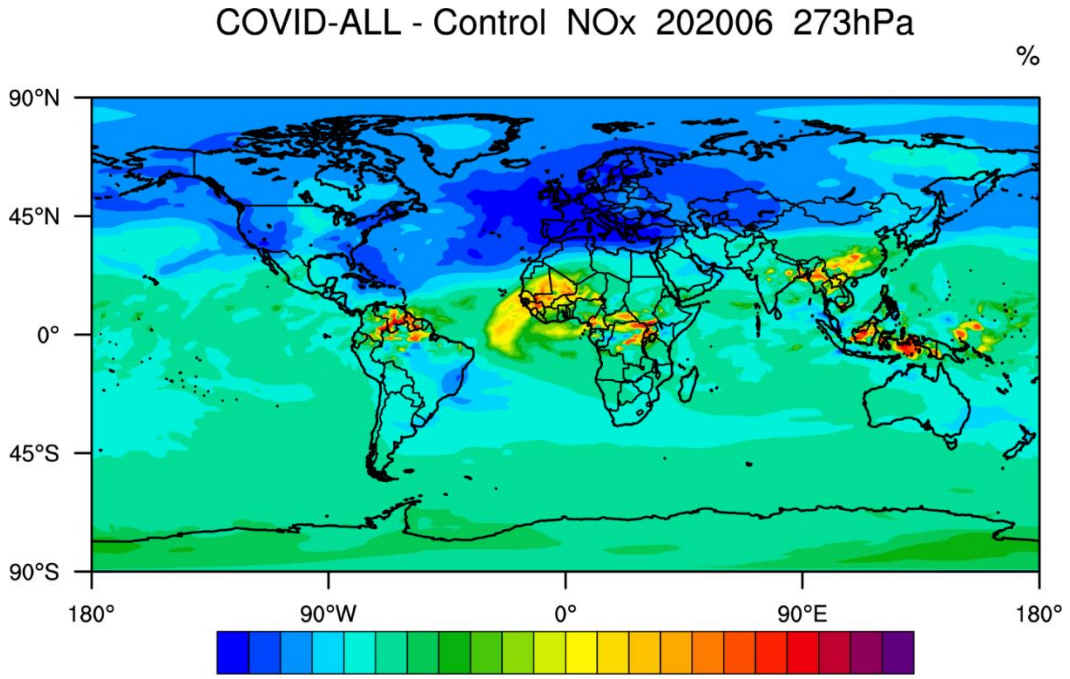

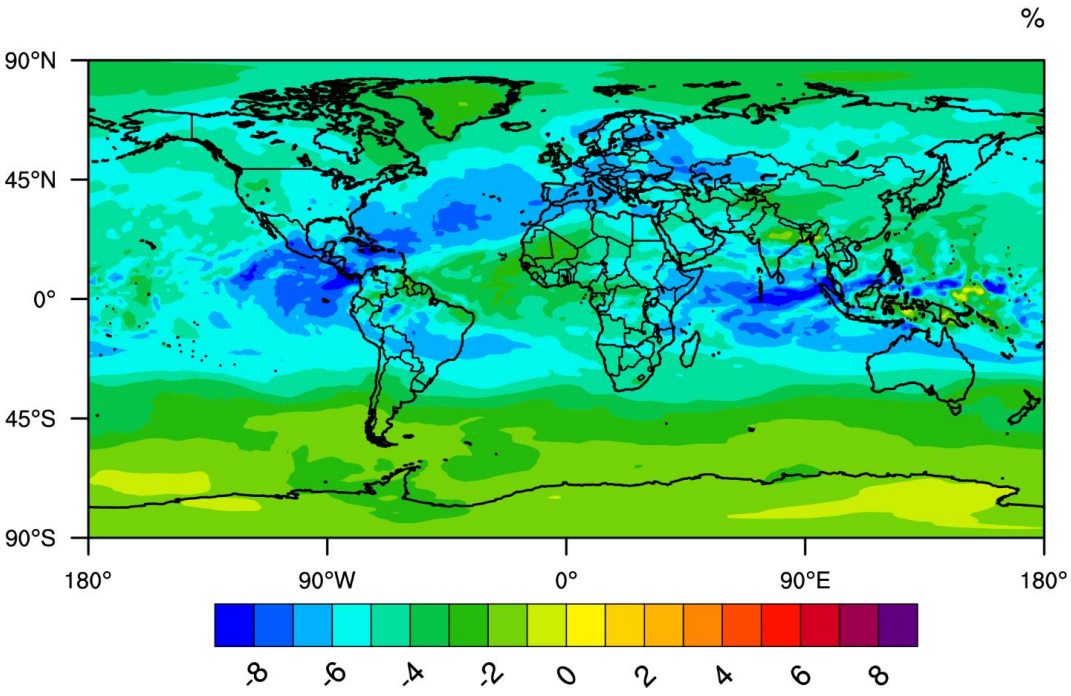

Figure S6. Relative changes (percent) in the monthly concentration of NO_x (top) and ozone (bottom) at the pressure height of 273 hPa (about 10 km or 32,000 ft) in response to the perturbations in the emissions of atmospheric pollutants during the COVID-19 pollutants. The changes at this altitude are affected mostly by the reduction in air traffic. The small positive NO_x changes in the tropics are due to the convective transport of positive surface anomalies due to enhanced residential activities.

Text S7. Effect of 2020 meteorological conditions

The influence of the dynamical inter-annual variability on tropospheric ozone is important and is analyzed by comparing the ozone fields calculated for 2020 (with and without COVID-19 effects on the emissions) with the model ozone climatology (cases 5 and 4). Our climatology is derived by averaging over the period 2001-2019 the seasonally evolving concentrations of the chemical species provided by our model simulation constrained by the MERRA-2 reanalysis.

We show in Figure S7 the percentage anomalies in monthly mean NO_x concentrations calculated in June 2020 respectively for baseline and for COVID-19 related conditions (surface and air-traffic perturbations) relative our adopted climatology (cases 4 and 5). The calculated distributions underline the large amplitude of interannual variations resulting from anomalies in atmospheric circulation, lightning-related NO_x formation and wildfire-related emissions. Based on the model estimates, NO_x should have been abnormally abundant in the free troposphere during 2020, particularly in the northern hemisphere (case 4, upper left panel). However, the perturbations in emissions due to the pandemic reduced the NO_x level in northern hemisphere and in the tropics (case 5, upper right panel).

Figure S7 also depicts the anomaly in the zonally and monthly mean ozone concentration in June 2020 derived for the baseline case 4 and the COVID-19 perturbed case 5, respectively relative to the 19-year climatology. As shown by Figure S7, the influence of the pronounced Arctic ozone depletion (300-100 hPa) on tropospheric ozone (500-300 hPa) poleward of 450N was substantial (case 4) and persisted near 250 hPa as late as the month of June, although with an amplitude considerably smaller than during springtime. In June, the influence of the springtime injection of stratospheric air with reduced ozone is still visible between 400 and 200 hPa poleward of 60°N (case 4, bottom left panel). The ozone concentration anomaly resulting from the perturbed emissions during the COVID-19 pandemic combined with the interannual variability (case 5) ranges from 5 to 15 percent north of 30°N. Averaged vertical profiles of the anomalies are provided in Figures S8 (polar latitudes) and S9 (hemispheric and tropical averages).

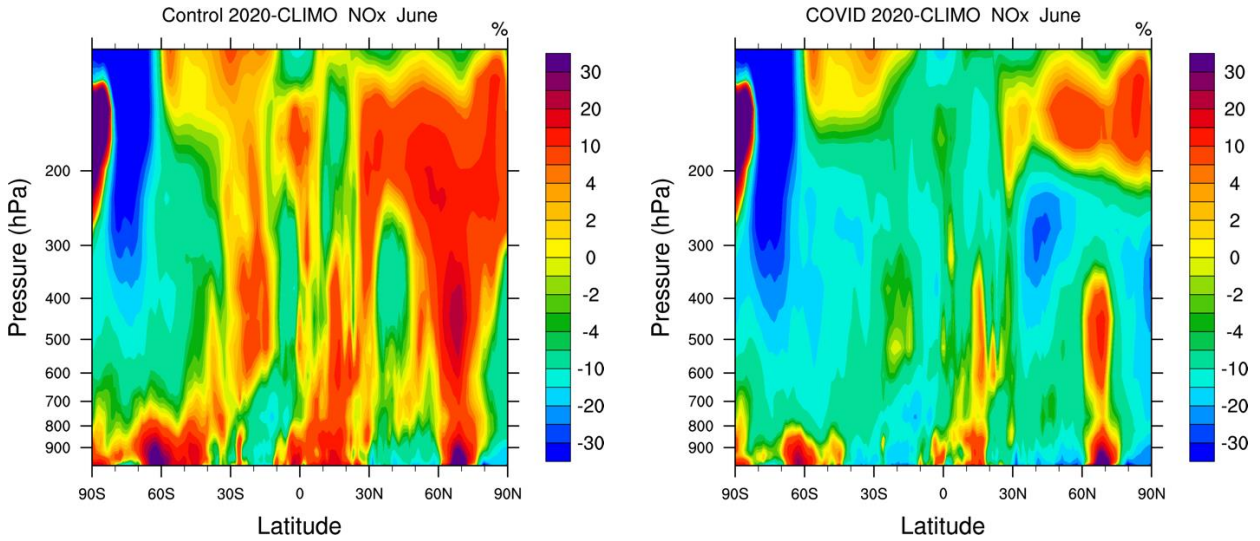

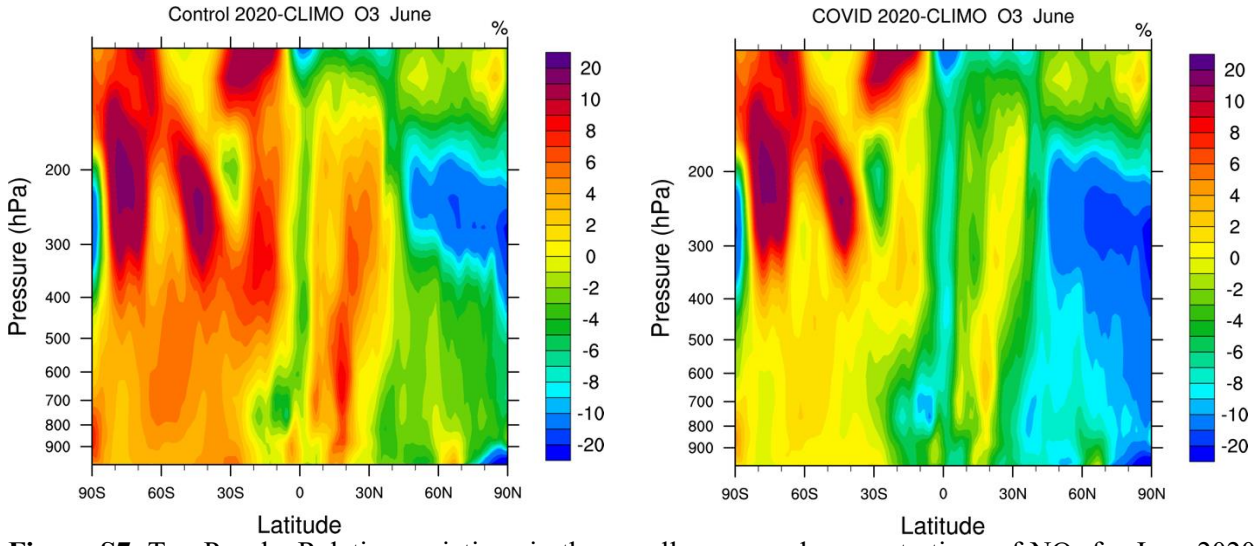

Figure S7. Top Panels: Relative variations in the zonally averaged concentrations of NO_x for June 2020 relative to 2001--2019 as a function of latitude and pressure for baseline conditions (left, case 4) and for COVID-19 situation (right, case 5). Lower panels: same as for NO_x in the upper panels, but for ozone.

Text S8. Vertical profiles versus climatology.

We show here the anomaly in the June 2020 monthly ozone concentration (with COVID-19 effects included) poleward of 65 degrees (south and north) relative to the 2001-2019 climatology. These results account for the effects of COVID-19 pandemic as well as for meteorological variability. The reduction in the ozone concentration for the combined case (case 5 with COVID-19 related changes in surface and air-traffic emissions) is of the order of 7 to 16 percent at high latitudes in the northern hemisphere and 2 to 3 percent at high latitudes in the southern hemisphere. These results, which account for the effects of meteorological anomalies in 2020, need to be compared with the results displayed in Figure S5 in which the effects of interannual dynamical variability are ignored (case 3). In both Figures S5 and S7, the largest reduction in ozone located near 250 hPa is attributed to the effect of the abnormal 2020 springtime meteorological conditions and ozone depletion in the Arctic lower stratosphere. The reduction persisted with decreasing intensity into the summer.

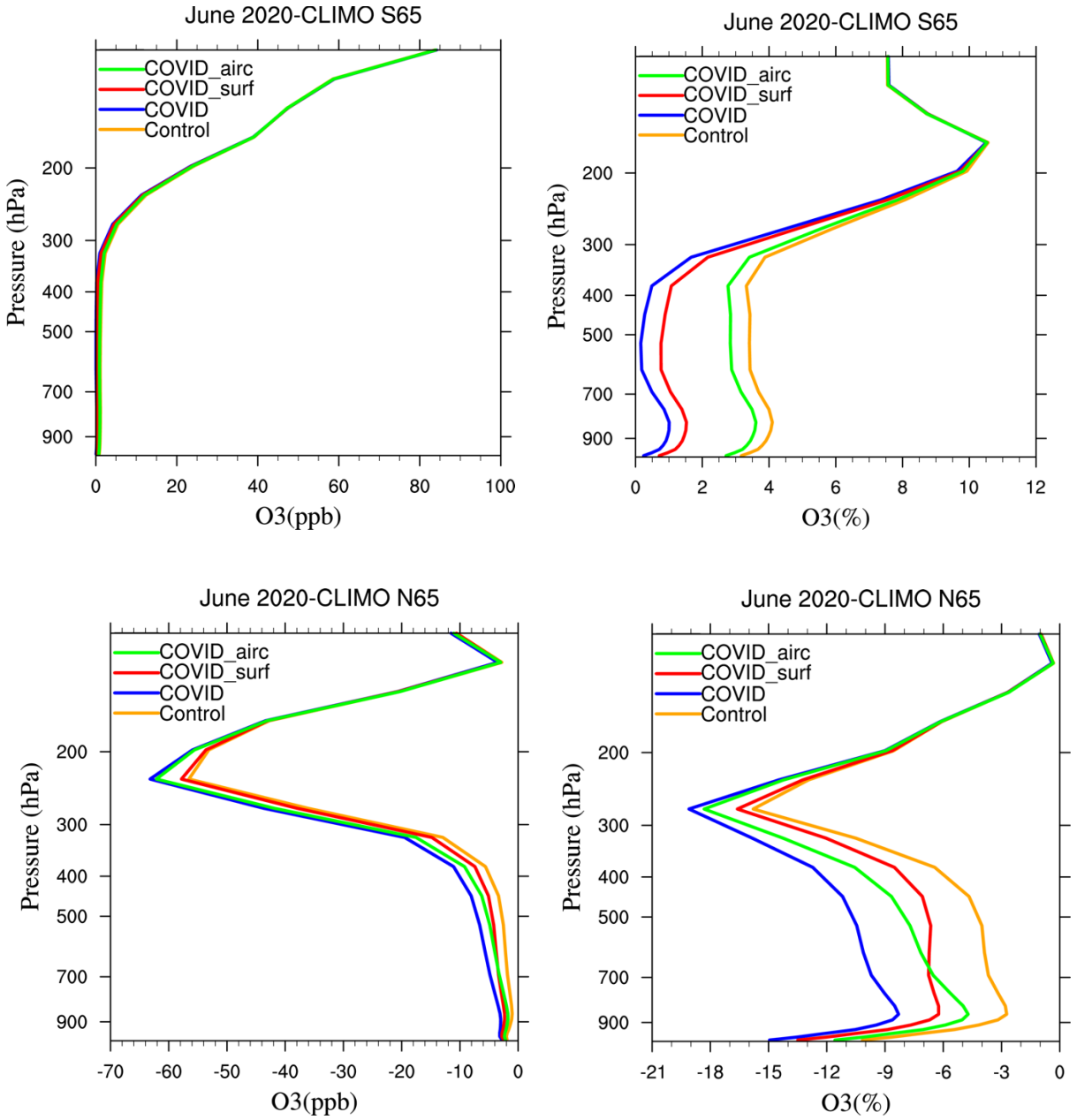

Figure S8. Vertical distribution of the June 2020 monthly mean ozone concentration anomaly (ppbv, left panels and percent, right panels) poleward of 650S (upper panels), and poleward of 650N (lower panels) due to COVID-related changes in surface (red curves, case 1) and aircraft emissions (green curves, case 2) relative to the 2001-2019 climatology. All combined effects are shown by the blue curves (case 5), which include the anomaly attributed to interannual meteorological variability and the influence of the large ozone springtime ozone depletion in the Arctic, represented by the orange curve (case 4).

Text S9.

We show here the anomaly (ppbv and percent) in the June 2020 monthly ozone concentration (with COVID-19 effects and meteorological variability included) relative to the 2001-2019

climatology averaged over the southern hemisphere, the tropics and the northern hemisphere, respectively. The reduction in the ozone concentration for the combined case (with COVID-19 related changes in surface and air-traffic emissions, case 5) between the surface and pressure height of 350 hPa is of the order of 2 percent in the southern hemisphere, 1 to 4 percent in the tropics and 6 to 9 percent in the northern hemisphere. The largest reduction in northern hemisphere ozone located near 250 hPa is attributed to the effect of the abnormal 2020 meteorological conditions and springtime ozone depletion that occurred during spring in the Arctic lower stratosphere and persisted with decreasing intensity into the summer.

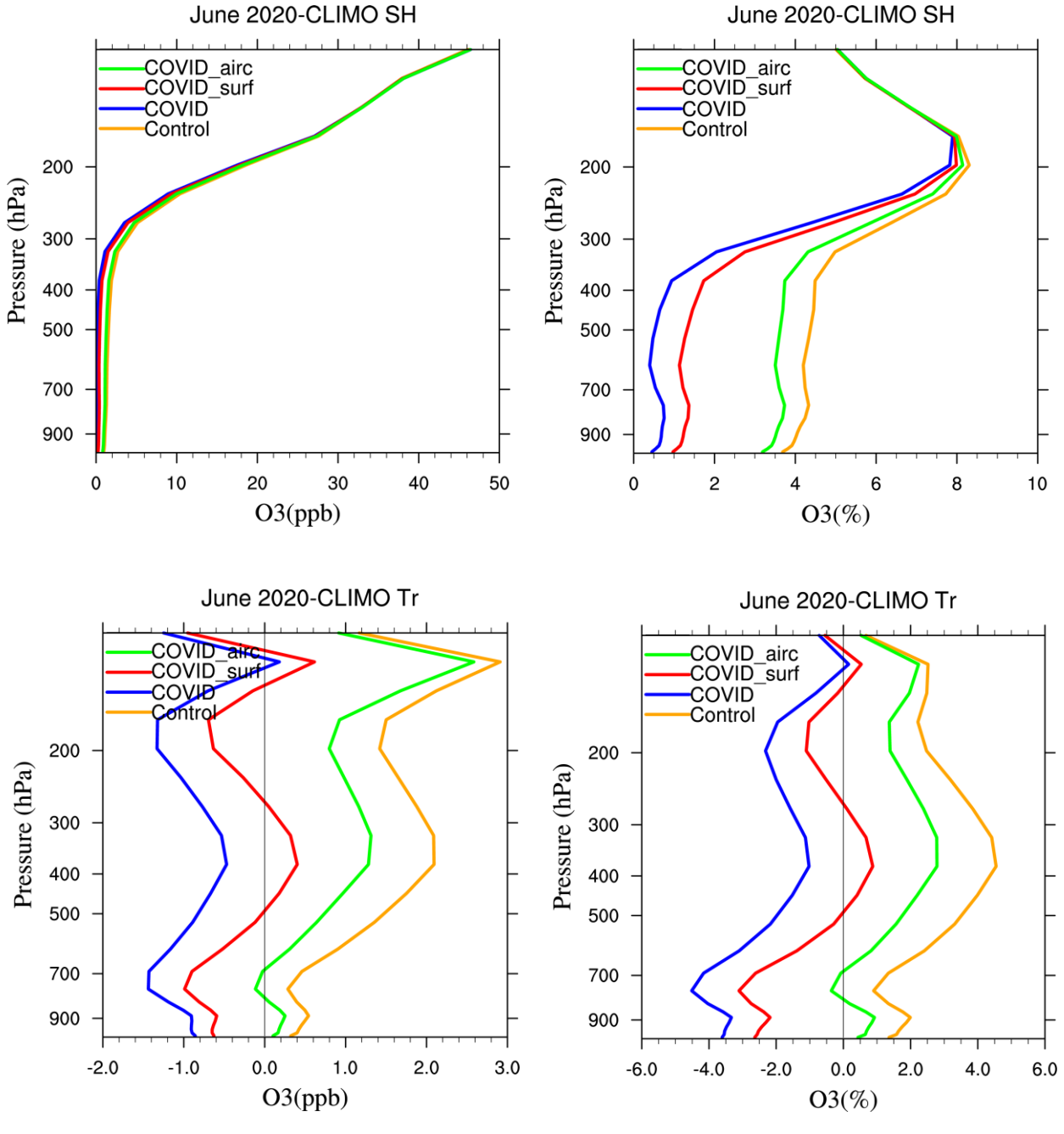

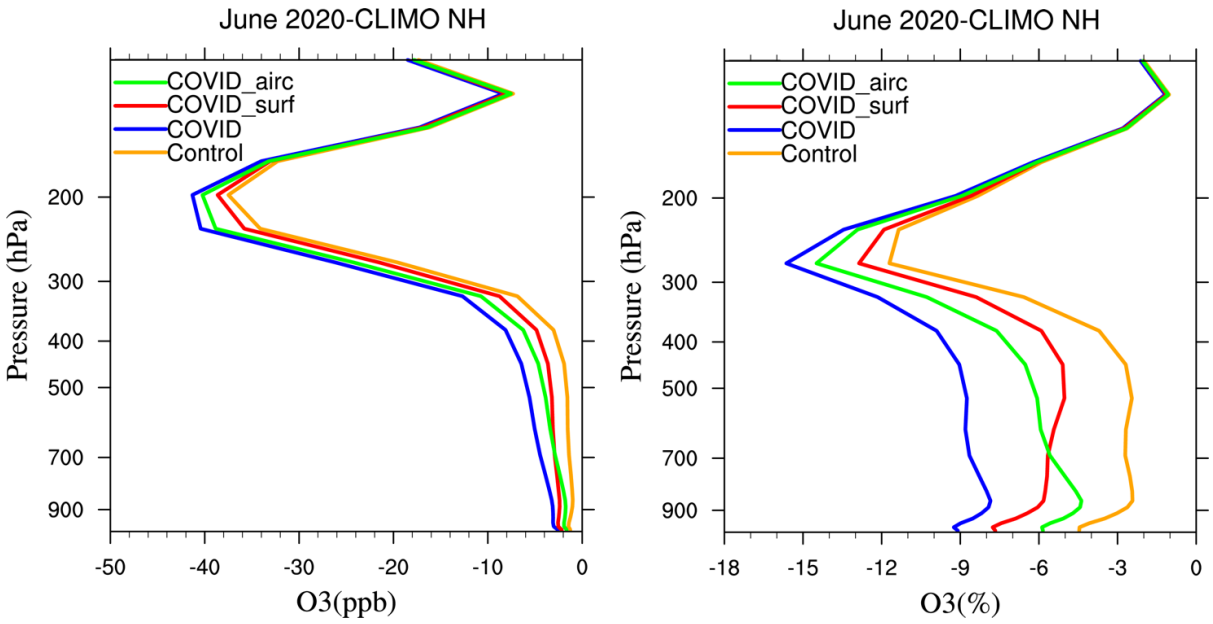

Figure S9. Vertical distribution of the June 2020 monthly mean ozone anomaly (ppbv, left panels and percent, right panels) for the southern hemisphere (upper panels), the tropics (middle panels) and the northern hemisphere (lower panels) due to COVID-related changes in surface (red curves, case 1) and aircraft emissions (green curves, case 2) relative to the 2001-2019 climatology. All combined effects are shown by the blue curves (case 5). These estimates account for the meteorological anomaly in 2020 relative to climatology. The orange curve shows the calculated anomaly resulting only from the interannual variability (case 4, meteorology including the effect of the abnormal ozone depletion in the springtime Arctic lower stratosphere)

Text S10.

Figs. S10 to S13 show the comparison of CAM-chem simulated ozone anomalies (case 5) with observed (case 5) and simulated anomalies (case 4, from the Copernicus Atmosphere Monitoring Service, CAMS) following Steinbrecht et al. (2021). Since the observations are only available at about 45 stations between 82°N and 54°S, the simulations are also considered at only the gridpoints next to these stations. Figure S10 shows the geographical distribution of the stations and of the observed and simulated ozone anomalies for spring and summer 2020. The 2020 tropospheric ozone anomaly is averaged from April to August and from 1 to 8 km altitude (~900 to 350 hPa), and is color-coded in the Figure. Since CAMS does not account for the 2020 emissions reductions (case 4), CAMS shows 5 to 10% higher ozone than observations and CAM-CHEM. The spatial distribution is similar in all cases: Due to contributions from 2020 meteorological conditions, including the large Arctic spring-time ozone depletion in the stratosphere, the largest negative tropospheric anomalies occur in the Northern Hemisphere, with no pronounced longitudinal structure.

a.)

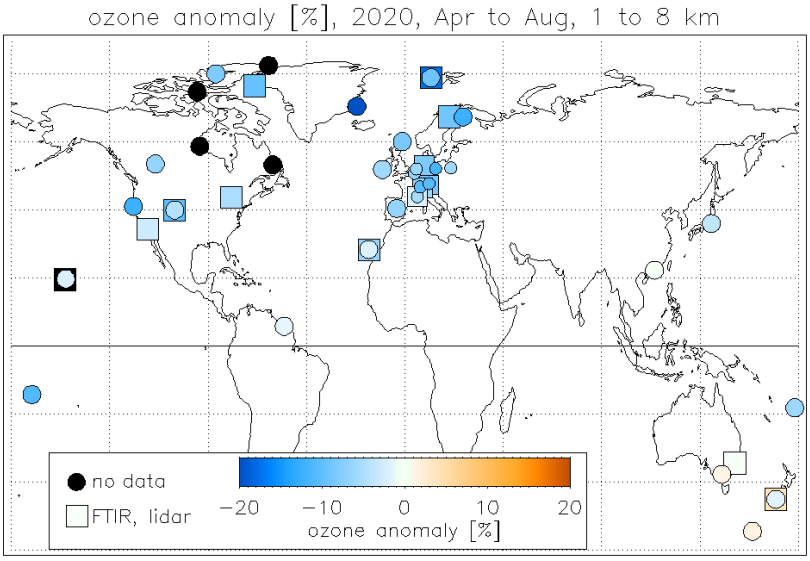

b.)

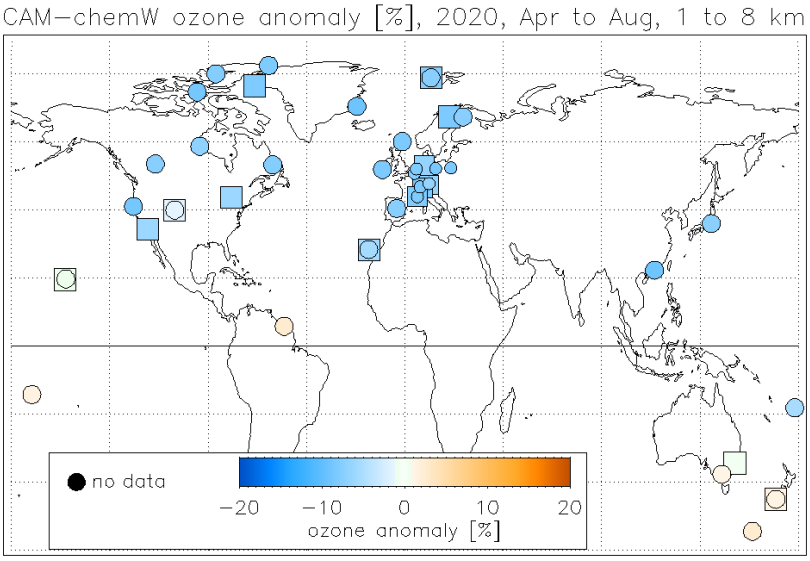

c.)

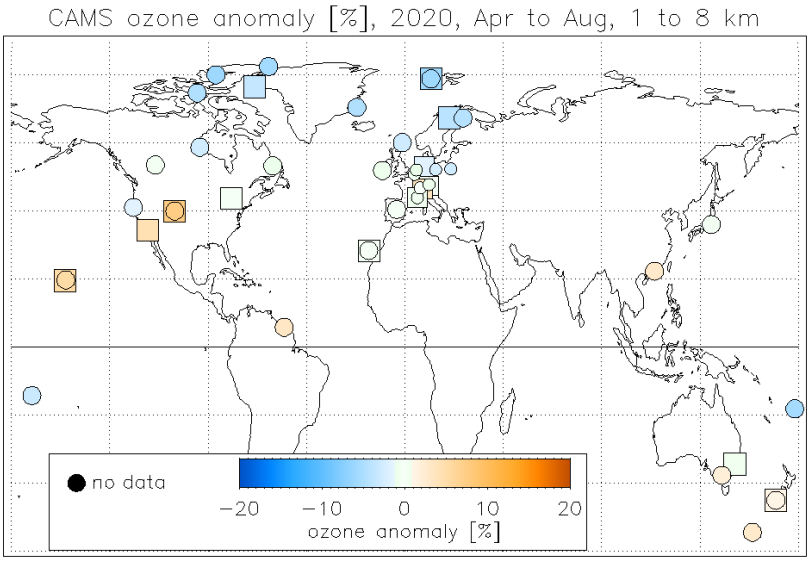

Figure S10. Stations used for comparing tropospheric ozone anomalies in 2020 between observations (panel a.) and simulations from CAM-chem (panel b, case 5, following Wilka et al. 2021) and Copernicus Atmosphere Monitoring Service (CAMS, panel c, case 4). Circles and squares show the locations of sonde, lidar and FTIR stations. Simulation data are taken at the corresponding grid-points. Colors give the average tropospheric ozone anomaly in 2020, averaged from April to August and from 1 to 8 km altitude (~900 to 350 hPa). Red colors indicate above average ozone in 2020, blue colors indicate ozone below average.

Text S11 to S13.

Similar to Figure 3, and extending Figure S10, Figures. S11 to S13 compare the simulated 2020 ozone anomalies (case 5) with observations and Copernicus Atmosphere Monitoring Service simulations (CAMS, case 4) from Steinbrecht et al. (2021). Anomalies are averaged over the stations in different latitude bands (compare station map in Figure S10). Since CAMS does not

account for the 2020 emissions reductions, CAMS shows higher ozone than observations and CAM-CHEM. For high latitudes, north of 65°N (Figure S11), meteorological conditions of 2020, including the large stratospheric springtime ozone depletion, are the major contributor to low ozone in 2020. Effects of reduced emissions are less pronounced at high latitudes, and appear mostly in summer below 500 hPa (~-5%), possibly also around 200 hPa, -5 to -10% due to air-traffic reductions. In tropics and Southern Hemisphere (Figure S12, S13), observations, CAM-CHEM simulations, and CAMS show similar meteorological ozone anomalies in 2020, with no indication of significant changes due to emission reductions in 2020.

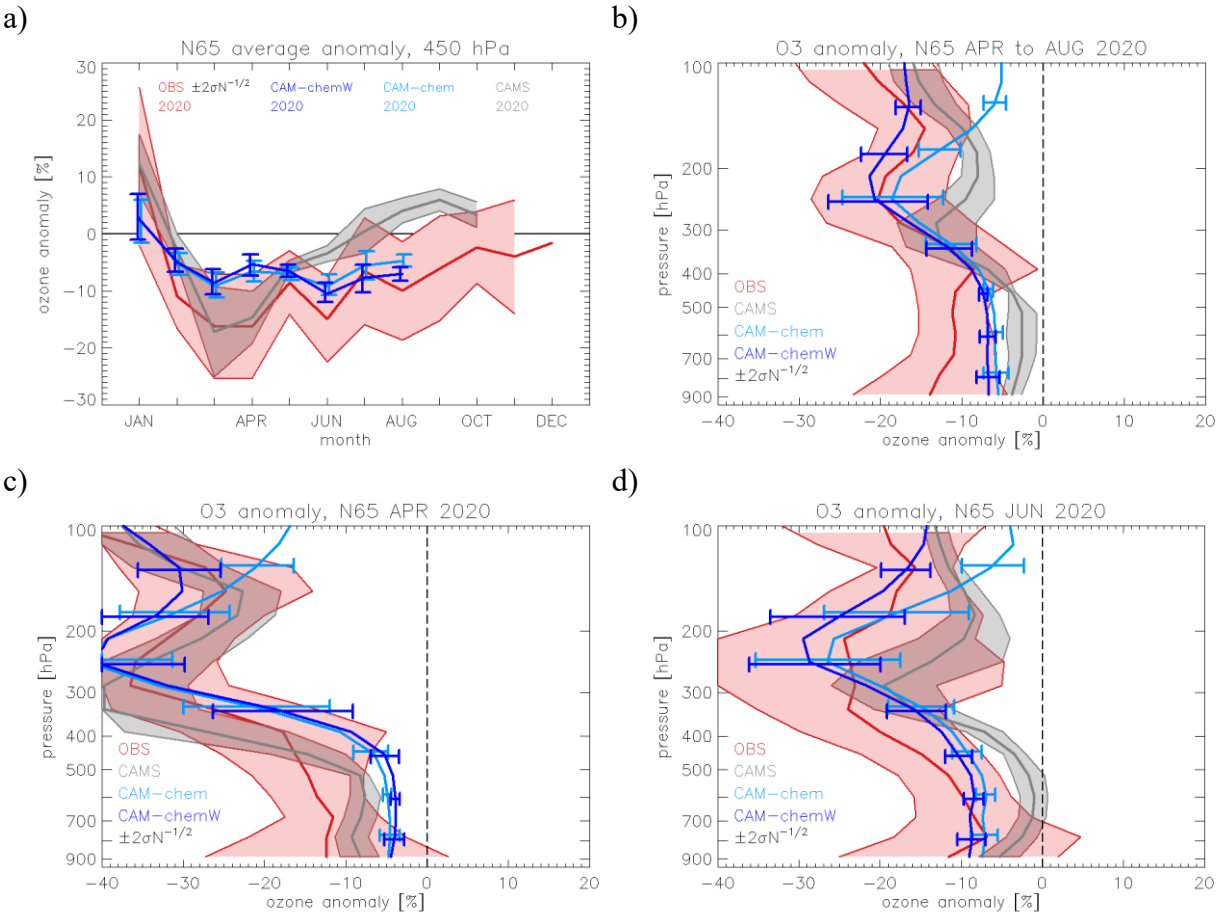

Figure S11. Panel a.) annual course of 2020 ozone anomalies at 6 km altitude (~420 hPa), averaged over all stations north of 65°N (see station map in Figure S10). Red: observations as in Steinbrecht et al. (2021). Light and dark blue: CAM-chem simulation (case 5), and CAM-chemW simulation with enhanced and more realistic Arctic stratospheric spring-time ozone depletion following Wilka et al. (2021). Grey: CAMS simulation (case 4). Panels b) to d): Profiles of the 2020 mean anomaly over all stations north of 65°N for April to August, April, and June. Error bars (or shading) give ±2 standard deviations of the mean over stations.

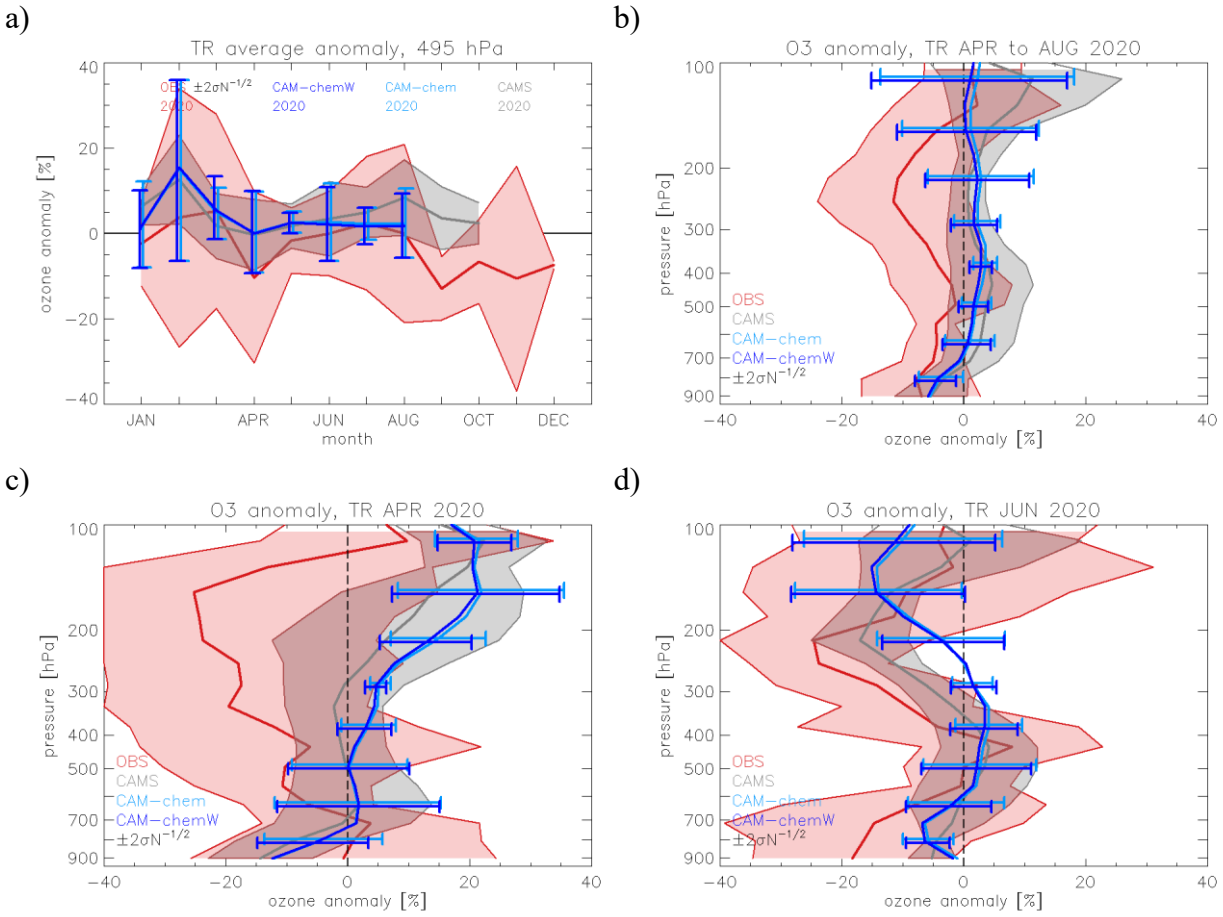

Figure S12. Same as previous Figure, but averaged over all tropical stations between 20°S and 20°N (see station map in Figure S10).

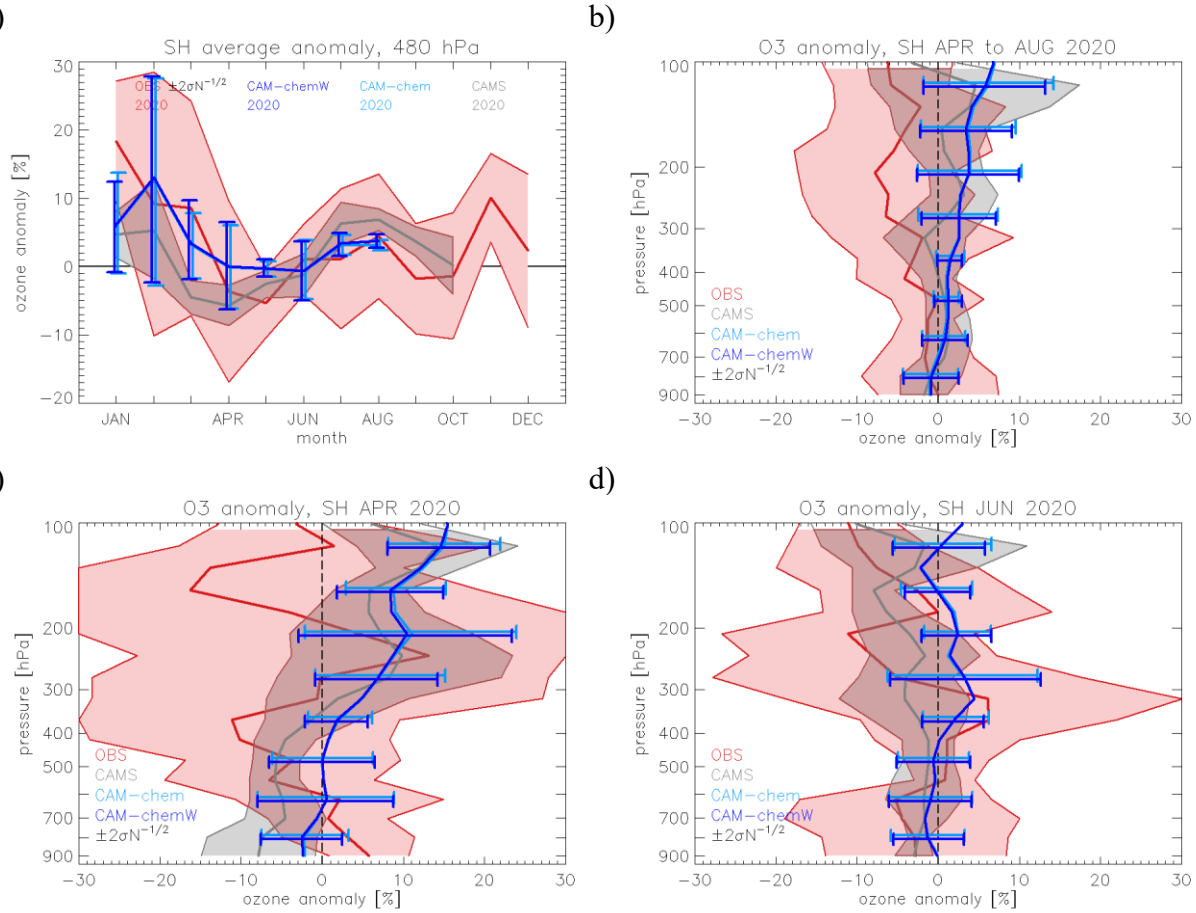

Figure S13. Same as previous Figures, but averaged over all Southern Hemisphere stations (see station map in Figure S10).